We are IntechOpen, the world's leading publisher of Open Access books Built by scientists, for scientists

6,900
Open access books available

185,000
International authors and editors

200M
Downloads

Our authors are among the

154
Countries delivered to

TOP 1%
most cited scientists

12.2%
Contributors from top 500 universities



WEB OF SCIENCE™

Selection of our books indexed in the Book Citation Index in Web of Science™ Core Collection (BKCI)

Interested in publishing with us?
Contact book.department@intechopen.com

Numbers displayed above are based on latest data collected.
For more information visit www.intechopen.com



Chapter 6

Applications of Strontium Aluminate Cements

The applications such as dense or thermal insulating refractory materials, the preparation of seawater resistance concretes and as the protection against X-ray and gamma ration are supposed for strontium aluminate cements [12,14]. The option to use strontium aluminate cement for the preparation of MDF composites as was described in Chapter 6.4 is also mentioned.

1. Refractory materials

Refractory products (**refractories**) possess the ability to resist high temperatures without physical or chemical destruction, the corresponding properties are termed as **refractoriness**. These materials can be classified according to their temperature resistance, chemical composition, porosity, etc. According to the most general viewpoint the ceramic and non-ceramic refractory materials and products can be recognized [423].

Based on the chemical composition, the following types of refractory materials can be specified:

- **Oxide ceramics:** are an extensive group of materials based on one or few oxides (SiO_2, Al_2O_3, Cr_2O_3, ZrO_2, MgO and CaO) and their stable compounds ($ZrO•SiO_2$, $MgO•Cr_2O_3$, $MgO•Al_2O_3$, $3Al_2O_3•2SiO_2$...). The silica refractory products, alumina-silica refractory products with different content of alumina, basic refractory products, alumina-zirconia-silica refractory products, alumina-chromic oxide-zirconia-silica refractory products, etc., are the most common examples of these materials. The alumina silicate refractories are extensively used in metallurgical, ceramic and glass industries. These materials are made primarily of refractory and kaolinitic clays, which are used both in crude and grog forms [424,425]. Spinel ($MgO·Al_2O_3$) is very attractive as refractory material in heavy industries because of its high melting point, low thermal expansion, considerable hardness, high resistance to chemical attack, favorable chemical stability, and good thermal spalling [426].
- **Non-oxide ceramics:** carbides (SiC[1] [427-429], B_4C [429-431], Al_4C_3 [432],...), nitrides (Si_3N_4 [433-435], BN [436], TiN [437], AlN [438], SiAlONs [439],...) silicides ($MoSi_2$ [440,441]) can be considered as the most common types. Among the physico-chemical properties of material the kind of applied bound is an important factor for these materials.

1 The formation of SiC was firstly described by Berzelius in 1810 and 1821, but silicon carbide was latterly rediscovered by Despretz, Schützenberger and Moissan. The preparation of SiC on a large scale was managed by Acheson is 1891 who named the new substance as carborundum [429].

INTECH
open science | open minds

© 2014 The Author(s). Licensee InTech. This chapter is distributed under the terms of the Creative Commons Attribution License (http://creativecommons.org/licenses/by/3.0), which permits unrestricted use, distribution, and reproduction in any medium, provided the original work is properly cited.

- **Other:** this type includes carbon or carbon containing refractory products such as Al_2O_3 – C [442,443], MgO-C [444], Al_2O_3-MgO-C [445,446], etc.

Another point of view for the classification of refractory products is the true porosity of refractory products:

- **Dense refractory products:** brick and castables of low porosity [447].
- **Insulating refractory products:** brick and castables of high porosity [447,448,498]. Insulating refractory castables are made of refractory light-weight aggregates, additives and HAC.
- **Ultra-light refractory products:** are refractory materials with true porosity higher than 75 %.

The morphology of refractory materials enables to recognize:

- **Shaped refractory products:** such as dense shaped refractory products, shaped insulating refractory products or fused cast refractory products.
- **Unshaped refractory products:** refractory castables for linings and reparations.

1.1. Regular refractory castable

The design of structures made of hydraulic–bound ceramics and subjected to high thermal stresses is of great importance today [449]. The development of refractory castables is important due to their increasing applications in metallurgical, cement and chemical industries. In last decades an increasing trend among refractories has arrived towards the replacement of bricks by castable refractories. Refractory castables can be classified on the basis of different aspects including the CaO content, the binder source, the chemical composition, the fluidity, the bulk density, etc. Their binding system plays a relevant role in different processing steps, including the workability, the dry-out and the service performance. Therefore, all efforts are made to improve the bonding agents [450-452,462].

The first reference on calcium aluminate bound refractory castables is provided by Deville [453], who prepared a refractory crucible using alumina aggregate and aluminate cement in 1856. Calcium aluminate cement and its industrial production was patented by Lafarge in 1908 [12,454] and the first industrial production was by Lafarge in 1913 and became known as "Ciment Fondu" [7,12,455]. Calcium aluminate cements are normally made by complete fusion of limestone or lime and bauxite or other aluminous materials with low content of SiO_2 at 1450 – 1600 °C. The molten clinker is tapped off continuously from the furnace, solidifies and its ground to the fines of about 3000 $cm^2 \bullet g^{-1}$. Their properties include rapid strength development, good resistance to sulfates and many other forms of chemical attack [7,12].

During the hydration of calcium aluminate as the main constituent of calcium aluminate cement, different hydrate phases can be formed. Up to 10 °C the hexagonal prisms of CAH_{10} (mono-calcium aluminate hydrate) are formed as the major product of hydration. The primary formed CAH_{10} converts to hydrogarnet (C_3AH_6), the only thermodynamically stable hydrate phase in the C-A-H system (Eq.1).

$$3\,CAH_{10} \rightarrow C_3AH_6 + 2\,AH_3 + 18\,H \quad (1)$$

$$3\,C_2AH_8 \rightarrow 2\,C_3AH_6 + H_3 + 9H \quad (2)$$

At temperatures above 10 °C, increasing amount of C_2AH_8 (di-calcium aluminate hydrate, strätlingite) is formed together with AH_3, while the content of formed CAH_{10} decreases. The conversion reactions (Eqs.1 and 2) are accelerated at high temperatures and moisture. The process is also associated with the strength loss and the formation of microcracks in the concrete structure. Above 27 °C the CAH_{10} hydrate is not formed at all and above 50 °C the C_3AH_6 is the only product of hydration. The hydration reactions of calcium aluminate can be summarized by the scheme in Fig.1. The hydration of ferrite phase is much slower than that of CA and $C_3(A,F)H_6$ is formed as the final product of hydration, with $C_2(A,F)H_x$ and $C_4(A,F)H_x$ as intermediates [7,12,415,456-460].

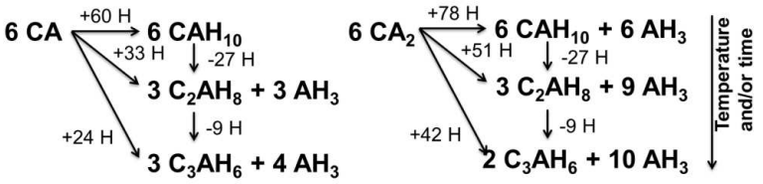


Figure 1. Hydration scheme of calcium aluminate cement [458].

Adding $CaCO_3$ to calcium aluminate cement induced the $C_3A \cdot CaCO_3 \cdot 11H$ hydrate formation (37 °C, samples immersed in water for 1 up to 30 days), inhibiting the formation/ conversion of CAH_{10} and C_2AH_8 metastable phases. Thus leading to better mechanical performance and dimensional stability. Moreover, although the mono-carbonate phase provides high mechanical strength to cement samples on the first day of curing, its decomposition combined with the C_3AH_6 and $Al(OH)_3$ generation due to continuous hydration of CA and CA_2 phases, seems to be one of the factors which lead to further improvement in compressive strength up to the 7th day [458].

CACs harden rapidly immediately after the massive precipitation of hydrates begins. Relatively high proportions of water are taken up in the hydration reactions, the theoretical w/c ratios needed for complete hydration of CA are 1.14, 0.63 and 0.46 for the formation of CAH_{10}, $C_2AH_8+AH_3$ and $C_3AH_6+2AH_3$, respectively [7,12]. The properties of the main hydrates are listed in Table 1. If the slurry of calcium aluminate cement is mixed with anhydrite (or gypsum), lime, bentonite or lithium carbonate (accelerator), the reaction is brisk and ettringite is the major product of hydration [599].

In monolithic refractories, calcium aluminate cement (CAC), one of the most widely used binders, promotes initial hardening and mechanical strength before firing. In the last few decades, the service life of alumina based refractory castables has been improved significantly by reducing the cement content. Carbon is not wetted by molten metal and does not melt,

Hydrate	Chemical composition [%]			Temperature	Crystalline structure	Density	Decomposition [°C]
CaO	Al_2O_3	H_2O	[°C]	[g·cm^{-3}]			
CAH_{10}	16.6	30.1	53.5	< 20	Hexagonal	1.72	120
C_2AH_8	31.3	28.4	40.3	20 - 30		1.95	170 – 195
C_3AH_6	44.4	27.0	28.6	> 30	Cubic	2.52	240 – 370
AH_3	---	65.4	34.6	> 30	Hexagonal	2.42	100

Table 1. Properties of hydrates formed in the strontium aluminate cement [460,461].

which is an excellent advantage for the refractory use. The reason for the cement content to be reduced is to prevent the formation of low melting temperature compounds in the presence of lime (CaO) [462-464].

Different types of binding systems have been developed (Table 2) throughout the years starting with hydraulic bonding, in which higher amounts of calcium aluminate cement (CAC) were used, towards coagulating binders such as colloidal silica or alumina [450,451]. In general, the refractory castables can be considered as composites, where the bonding phase (matrix) is reinforced by particles of aggregate (reinforcement) [465,480].

Nevertheless, there are some drawbacks related to the use of CAC in the systems containing microsilica and/ or magnesia, as the presence of CaO coupled with these other oxides results in the formation of low melting point phase at high temperatures. Other important concerns for cement-based castables arise during the curing and dewatering steps, which must be performed carefully in order to reduce the explosive spalling probability. In order to minimize these drawbacks, the properties of the refractory castables were improved by decreasing the cement content [111,450,466,470].

Based on the content of cement, the following types of refractory castables are defined by ASTM C401-91 (Standard Classification of Alumina and Alumina Silicate Castable Refractories):

- Normal Cement Refractory Castable (NCCs) or Conventional Cement Castables (CCs) where the content of CaO > 2.5 %.
- Low Cement Refractory Castable (LCCs) where 2.5 > CaO > 1.0 %.
- Ultra-low Cement Refractory Castable (ULCCs) where 1 > CaO > 0.2 %.
- No-Cement Refractory Castable (NLCCs) also Zero Cement Refractory Castables (ZCCs) or Cement Free Castables (ZFCCs).

Another way often applied for the classification of refractory castables is based on the density and the bonding system (see Fig.2) [455].

Bond type	1920s	1930s	1940s	1950s	1960s	1970s	1980s	1990s	2000s	2010s →
Hydraulic bond *Based on hydraulic setting and hardening*	Conventional cement bonded castables (Silicate cement, low purity CA cement)									
					Pure CA cement bonded castables (CA cement with improved purity)					
							High purity CA cement bonded castables (High purity CAC + uf.-Al_2O_3)			
							ρ-Al_2O_3 bonded castables			
								Hydratable Al_2O_3 bonded castables.		
Chemical				Phosphate bonded castables (H_3PO_4 or $Al(H_2PO_4)_3$ + MgO or CA) Water glass bonded castables ($Na_2O{\bullet}nSiO_2$ + Na_2SiF_6)						
					Sulfate, chloride bonded castables ($Al_2(SO_4)_3$ + CA, $MgCl_2$ or $MgSO_4$)					
Polymerization					Polyphosphate bonded castables ($Na_5P_3O_{10}$ or $(NaPO_3)_6$ + MgO, CaO or CA)					
							Resin bonded castables (Phenol resin, Novalac resin + cross linker)			
Hydraulic + coagulating						Low cement castables (CAC + Clays, CAC + uf.-SiO_2)				
Coagulating						Clay bonded castables (CA + Ca-, Na-clay)				
							Ultralow cement castables (uf.-SiO_2, uf.-Al_2O_3 + CA) Non-cement castables (uf.-SiO_2, uf.-Al_2O_3 + electrolyte, uf.-SiO_2 + MgO)			
							Sol bonded castables (silica sol, alumina sol + electrolytes)			
Carbon bonded								MgO – Carbon Castables		
Nano-engineered										In progress

Table 2. Progress in binding system for refractory castables [451].

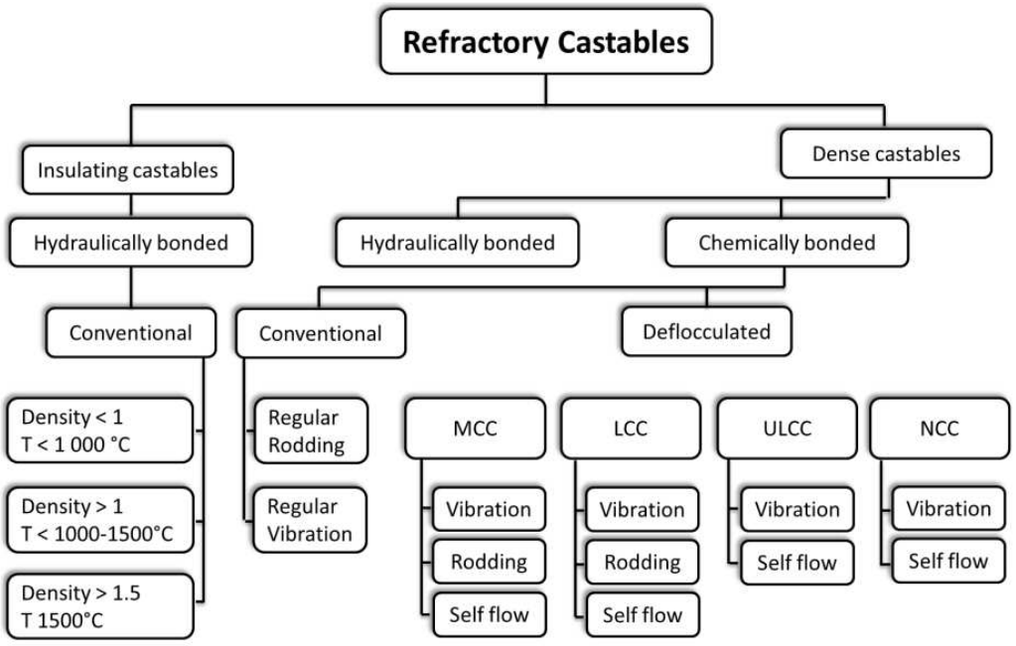


Figure 2. Types of Refractory Castables [455].

Calcium aluminate cement acts as a suspension lubricant and binder in fresh mix and after hardening in room temperature it provides the strength. Cement castables (CCs) are usually porous and open textured, due to relatively large amounts of water required for the hydration of AC. They also exhibit a characteristic drop in strength at intermediate temperatures as sluggish sintering does not allow the development of ceramic bond after breaking down the hydraulic bond. Furthermore, high content of lime in these castables favors the formation of low melting phases such as anorthite and gehlenite at elevated temperatures. These phases are known to degrade the refractoriness and corrosion resistance of conventional CCs [111,466].

Especially low-(LCC) and ultralow-cement castables (ULCC) are widely used in steel industry due to their superior rheological and physical properties. Initially, castable refractories were composed of only cement and aggregates. Then, the addition of deflocculants and fine fillers has followed with the aim to optimize and control the properties such as workability as a function of time [463]. Such castables have valuable properties, including low thermal expansion coefficient, good thermal conductivity, good thermal shock resistance, high resistance to slag and liquid metal corrosion and high strength at low and high temperatures. ULCC refractories have strong slag penetration resistance [462].

Different calcium-free binding systems such as hydratable alumina (HA), colloidal silica (CS) and colloidal alumina (CA) were developed for the refractory castables. Hydratable aluminas (HA) are amorphous mesophase transition aluminas (TA)[2] which are produced by flash

2 Transition aluminas are described in Chapter 4.1.

calcination of gibbsite in the temperature interval from 400 to 800 °C[3], which leads to high specific surface area transition phase of ρ-alumina (rho-alumina) [486,450,467-470].

The binding ability of ρ-alumina derives from its particular characteristic while undergoing the rehydration when in contact with water (or water vapor). During the hydration, a thick layer of gel is formed, a part of the gel subsequently crystallizes into traces of boehmite and major quantities of bayerite. The remaining gel phases were identified as boehmite gel or pseudo-boehmite (a poorly crystallized boehmite), together with totally amorphous gel, and may represent up to 60% of final hydrated phases, depending on the hydration temperature and pH. Interlocking bayerite crystals and gel confer the mechanical strength to green body of the refractory structure by filling pores and interfacial defects and by forming the honeycomb structures on the surface of aggregates attaching adjacent grains to each other and to the surrounding matrix [450,470,471].

The process of TA (transition aluminas) rehydration in Hydratable Alumina-bonded Refractory Castables (HAB)[4] can be expressed by the following reaction scheme [471,472]:

$$TA + H_2O \rightarrow \text{amorphous gel} \rightarrow \text{pseudoboehmite} \rightarrow \text{boehmite} \rightarrow \text{bayerite} \tag{3}$$

The hydration process can be divided into four stages [458]:

1. The intensive period of preliminary hydration.
2. The induction period.
3. The acceleratory period, in which the maximum speed of evolving heat is attained. The crystallization of amorphous gel phase and the formation of bayerite as well as the changes in the morphology of grains proceed in this period.
4. The final period, where the amount of released heat decreases asymptotically.

Although hydratable aluminas outweigh the low-melting point phase generation associated with microsilica-containing CAC-bonded castables, there are still some drawbacks attributed to this binder. Compared to equivalent CAC formulations, HA-bonded castables require longer mixing time and high water contents due to high specific surface area of the binder. Moreover, after hardening, HA-containing castables form much less permeable structure in comparison with CAC bonded castables, which leads to higher explosive spalling probability during the water dry-out [450].

A great concern has been employed during recent years to refractory castables bound by nanopowders and colloidal suspensions in order to improve the refractory's bonding and densification and the behaviour during sintering. Therefore the addition of nano-particles could improve the castable properties, as long as the nano-agglomeration problem is kept under

3 The process is commonly used for the production of catalysts, carriers and absorbents.

4 Usually prepared by flash calcination of gibbsite.

control. High price of commercially available nano-powder products can also be a hindrance. Thus, nano-particles containing aqueous suspensions (colloidal binders) are preferred to nano-powders [450].

Among colloidal suspensions, the silica sol is of greatest interest for refractory castable applications. One of the reasons for its use is the possibility of mullite formation at low temperatures for alumina-rich systems. Actually, the reaction activity of nanoSiO_2 particles in silica sol is extremely high. Colloidal particles can be absorbed on the surface of active α-Al_2O_3 ones and fill in their packing gaps, which can reduce the temperature of mullite formation, with suitable densification at about 1100 °C. Another reason for applying colloidal silica to refractory castables is related to its high solid contents, ranging from 15 to 50 wt. % of silica [450].

The fact of increasing the utilization of colloidal silica as a binder has initiated a discussion concerning the possibility of adding colloidal alumina for the same purpose. Despite the colloidal silica advantages, its addition always implies that SiO_2 will be present in the final product, which would inhibit its use in various steel plant applications. This drawback was the driving force towards using colloidal alumina. At first, the addition of colloidal alumina was restricted to the contents lower than 1wt %, most likely due to processing difficulties such as high water demand and low flowability and workability. However, after overcoming these limitations, recently higher colloidal alumina solid contents (up to 4 wt. %) could be added to the refractory castables. For lower solid contents in the composition, the role of colloidal alumina as a binder may be insufficient whereas if it exceeds 4 wt. %, higher water amounts are required for mixing and the mechanical properties may be spoiled [450].

In addition to colloidal silica and alumina, there is also a report related to the utilization of mullite and spinel sols (Fig.3(a)) as bonding agents in high alumina ULCC castables [450,473,474]. These sols with low solid content (about 5 wt. %) in water suspension were prepared by the addition of silica fume and $MgCl_2$ $6H_2O$ into vigorously stirred boehmite sol (Fig.3(b) and (c)) and used as an additive for CAC containing castables in order to evaluate their effect on physical and mechanical properties, as well as on slag corrosion and thermal shock resistance. The microsilica content in a spinel bound high alumina castable must be reduced to a very low level to eliminate the detrimental glassy phases or the formation of SiO_2-Al_2O_3 melt at the temperatures close to 1250 °C [475,478].

The spinel additive from the sol–gel route contained more fine particles and showed better performance in castables than co-precipitated spinel additive, although both of them are energetically favorable to produce desired spinel phases at lower temperature but with significant volume expansion. The magnesium aluminate spinel (MA, $MgAl_2O_4$) is a very desirable phase in castables which improves the hot strength, the creep resistance, the thermal stability and restricts slag penetration of spinel containing castables [474,476,477,480].

Alumina-magnesia castables are widely known for their expansive behaviour, due to in situ formation of $MgAl_2O_4$ at temperatures higher than 1000 °C. CAC-containing alumina-magnesia castables performed better regarding the mechanical strength and thermal shock resistance. Nevertheless, they attained higher in situ expansion, due to the CA_6 formation

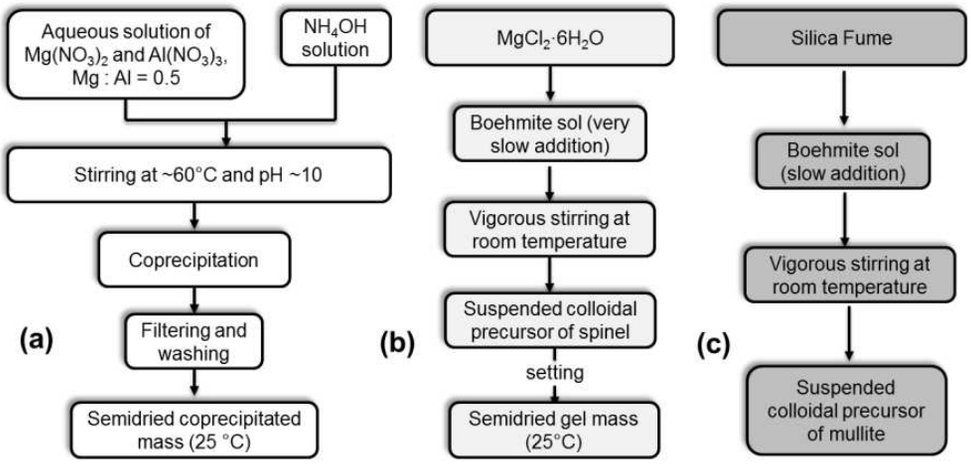


Figure 3. Preparation of co-precipitated spinel (a), sol-gel derived spinel (b) and mullite (c) [473,474].

during the thermal treatment. An efficient way to control the volumetric stability can be achieved by the addition of hydratable alumina, as its shrinkage behaviour counterbalances the in situ spinel expansion. Furthermore, this binder leads to higher creep resistance and also low apparent porosity levels, which can be useful to reduce the slag infiltration [445,478,479].

Self-flow refractory castables (SRFC) are characterized by their consistency after mixing, which allows them to flow and de-air without the application of external energy, i.e. vibration. Added water promotes the flowability of the particulate system but it has to be kept at minimum dosage (typically between 3 and 8 wt.% in conventional castables), to avoid coarse particles segregation and the increase in final porosity. In order to compose the Self-Flow Refractory Castable, the deflocculants and the particle size distribution of aggregates have to be selected carefully since the particle size distribution is one of the most important factors that affect the refractory's rheological properties [480-482].

The reliability of linings and pieces of refractories used in vessels (ovens, converters and ladles) must also be ensured because these structures are subjected to high temperatures under normal conditions. Previous studies were undertaken to model the thermo-mechanical behaviour of concrete and refractories. For these materials the temperature range of 20-800°C is of particular interest because, due to the dehydration, the cement undergoes significant microstructural transformations during the first thermal load [111,449].

These transformations considerably modify the thermo-mechanical behaviour of the material and must be taken into account for a realistic structural analysis. The chemical reactions may be described by the following equations [449]:

$$AH_3 \rightarrow AH+2\,H \tag{4}$$

$$AH \rightarrow A+H \tag{5}$$

$$C_3AH_6 \rightarrow C_3AH_{1.5} + 4.5\,H \tag{6}$$

$$C_3AH_{1.5} \rightarrow \left(C_{12}A_7, CA, CA_2, CA_7, A\right) + 1.5\,H \tag{7}$$

The hydrogarnet phase C_3AH_6 is decomposed into two phases $C_{12}A_7H$ and CH, the chemical condensed formula of which is $C_3AH_{1.5}$. Therefore it should be written [457,483]:

$$7\,C_3AH_6 \rightarrow C_{12}A_7H + 9\,CH + 32\,H \tag{8}$$

Growing demand for refractory castables with designed properties has brought about continuous technological development involving the simultaneous understanding of particle size distribution, the use of additives improving workability as well as sintering additives and the binder performance [484].

1.2. Particle packing density

Particle packing density (PSD) was evaluated by the Andreasen model [463,480,485,486]:

$$CPFT = 100 \times \left(\frac{D}{D_L}\right)^n \quad [\%] \tag{9}$$

where ***CPFT*** denotes the cumulative percent of grains finer than ***D***, $\boldsymbol{D}_L$ is the size of maximum used grain, ***D*** means the grain size and ***n*** is the particle size distribution parameter.

Another packing model is proposed by Dinger and Funk [485,487]:

$$CPFT = 100 \times \left(\frac{D^q - D_S^q}{D_L^q - D_S^q}\right) \quad [\%] \tag{10}$$

where $\boldsymbol{D}_S$ and $\boldsymbol{D}_L$ are the smallest and largest particle sizes, respectively. The parameter ***q*** is the coefficient, which depends on the particle size distribution.

Despite the fact that water is used in rather small amount (usually 3 – 8 % in convectional refractory castables), it still remains the key ingredient that enables to keep the desired rheological characteristics of fresh castable (Fig.4). Since water fills the voids between solid particles first, improving the packing density is an obvious way to reduce the water requirement. The workability can be improved by external vibration but when it is not possible or advisable, self-flow refractory castables (SFRC) are used. SFRC "works" as a suspension of powders in which the fine matrix is the flow medium that envelops the aggregate particles, fills in the voids between them and suspends them, promoting higher flowability [486-489].

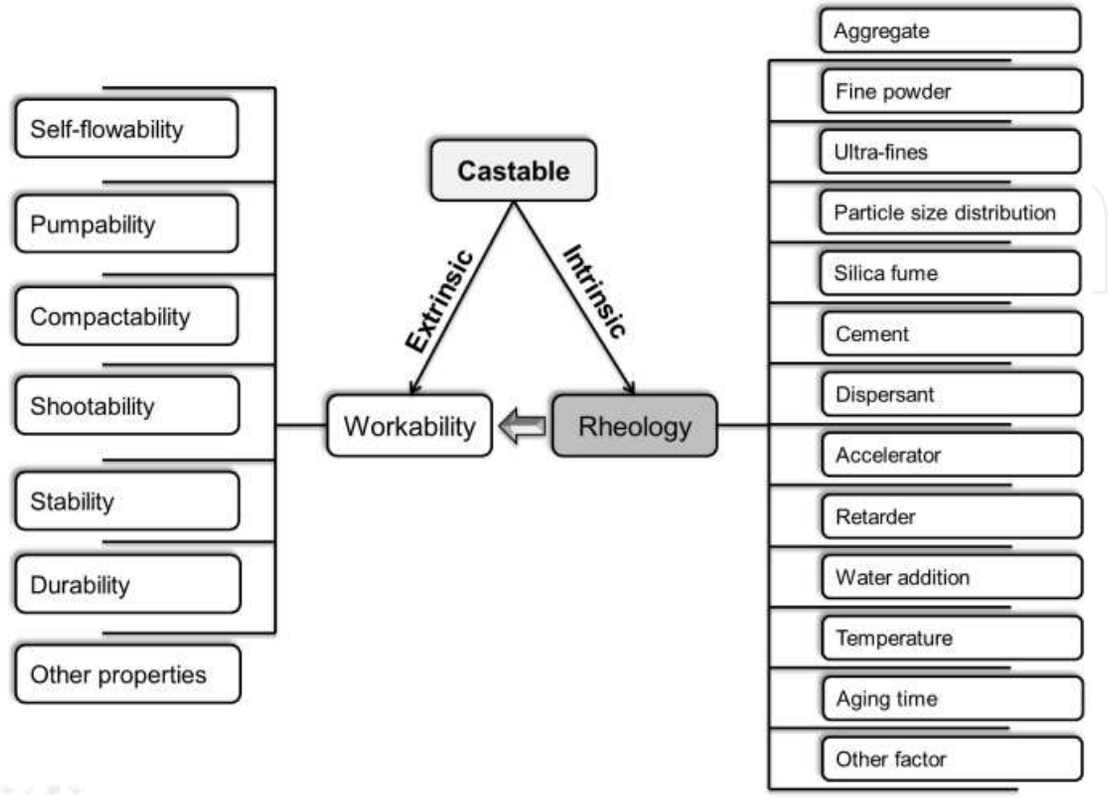


Figure 4. Factors influencing the rheology of castables [489].

1.3. Opening material

Opening material (aggregate) and filler usually improve the drying and firing shrinkage, the material mechanical properties, the thermal stability, the corrosion resistance and the thermal conductivity of refractory materials. Dense refractory castables from alumina-silica system often use corundum or calcined bauxite [110,131,463], mullite [484], refractory clays [423,490] or sand [491]. Moreover, the aggregates such as SiC [464,492,493] or zircon [494,495] are used.

1.4. Sintering additive

The use of boron-based sintering additive to speed up the refractory densification at lower temperatures can be a suitable alternative to develop novel compositions for fluid catalytic convertors (FCC) of petrochemical units [484]. Cr_2O_3 nanoparitcles are effective sintering additive for MgO based refractories due to the formation of $MgCr_2O_4$ spinel. The layer of spinel precipitates at the grain boundaries of MgO grains [496]. The addition of SiO_2, $CaCO_3$, TiO_2 and Y_2O_3 also improves the densification of refractories based on $MgCr_2O_4$ spinel [497].

1.5. SrAC bound refractory castable

Refractory castables based on strontium aluminate cement can be prepared by mixing strontium aluminate cement, grog (Chapter 6.1.3) and additives (Chapter 5.4). The increase of Al_2O_3 content in the castable by the addition of corundum or calcined bauxite (Fig.3 in Chapter 2) shifts the equilibrium composition towards the high alumina phases (Fig.1 in Chapter 1.2) such as calcium dialuminate and calcium hexaaluminate. Build line or casted panel is less sensitive to humidity, because newly formed strontium aluminate phases are much less reactive after mixing with water (Fig.12 in Chapter 5) than original strontium aluminate cement.

Optical and electron microscopy of prepared refractory castable based on strontium aluminate cement is shown in Fig.5 and Fig.6, respectively.

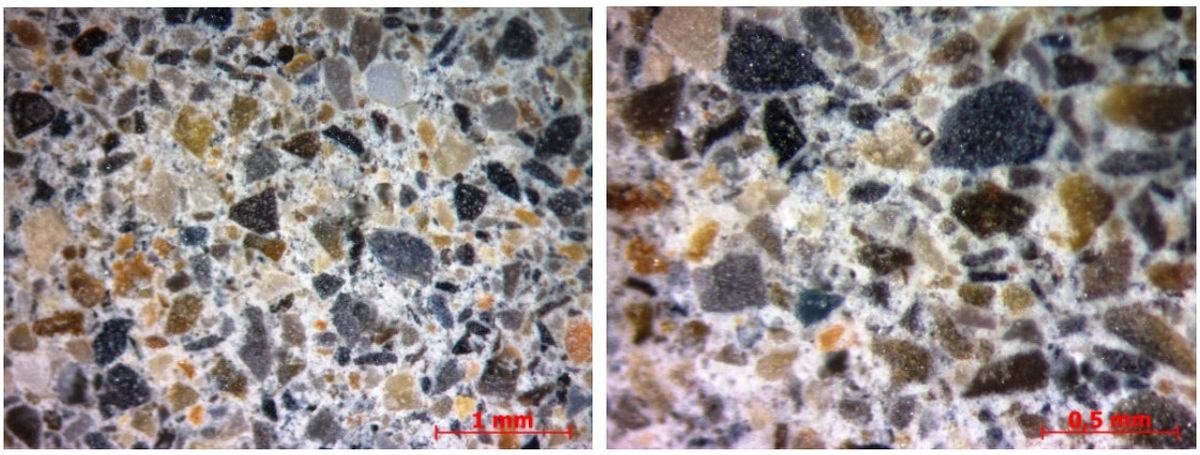


Figure 5. Optical microscopy of texture of SrAC bound refractory castable with bauxite aggregate.

The sample fired to the temperature of 1300 °C shows zero total shrinkage[5], therefore the castable has sufficient temperature stability that is necessary in order to avoid cracks formed during drying and further thermal treatment.

The texture of fired sample is shown in Fig.7. The texture of the material shows hexagonal plates, which are the pseudomorphosis of original hydrates. These hydrates are already decomposed at temperatures lower than 600 °C (please see Fig.5 in Chapter 5). Moreover, the excess of Al_2O_3 from applied aggregate (calcined bauxite) changes the equilibrium composition as was discussed above. Some sites show the initial stage of sintering process, i.e. the formation of necks between neighboring particles, and newly formed phases nucleating from the melted zone.

5 Total shrinkage consists of the change of specimen dimensions during setting, drying and thermal treatment.

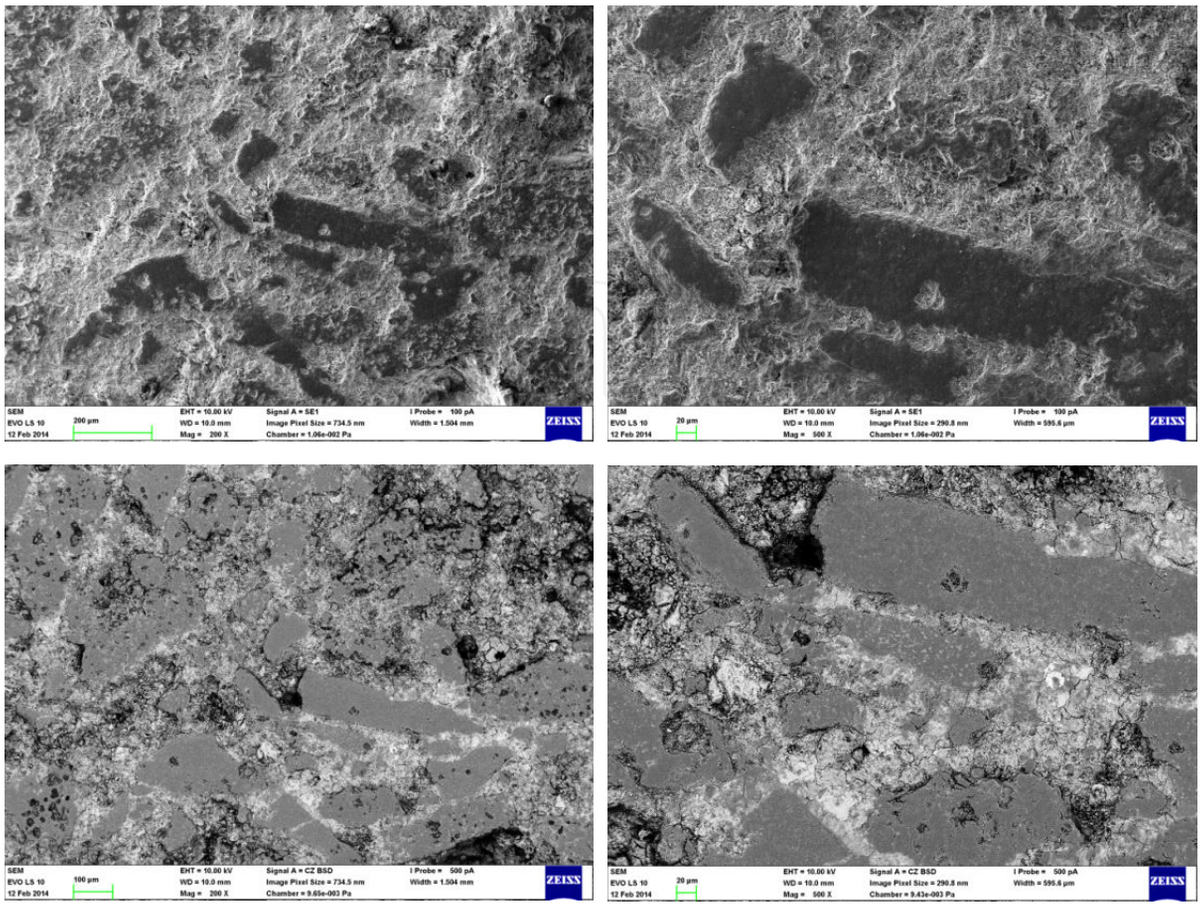


Figure 6. Electron microscopy of refractory castable before the thermal treatment.

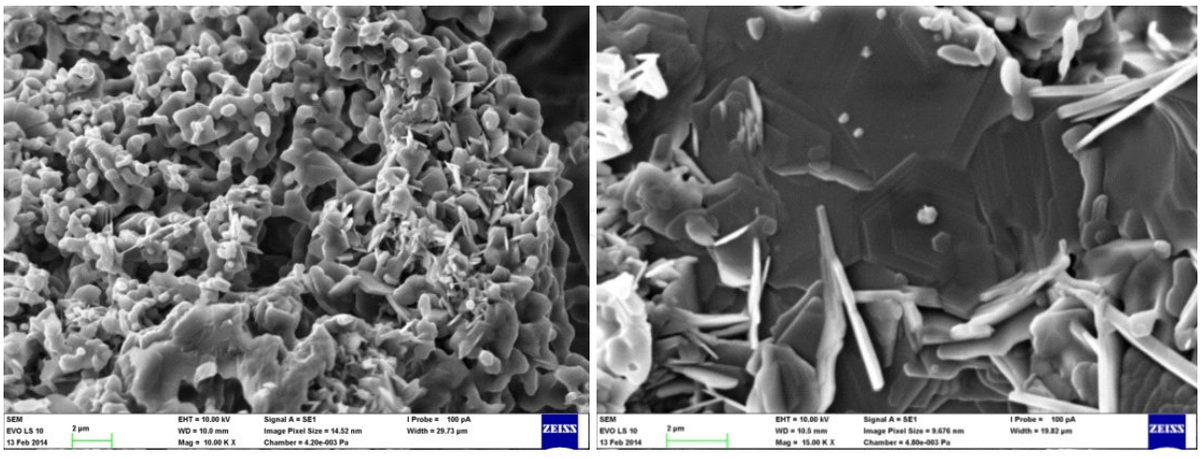


Figure 7. Electron microscopy image of refractory castable treated to the temperature of 1300°C.

The recrystallization or better sinter-crystallization takes place in the material treated to the temperature of 1400 °C (Fig.8). The process is connected with increasing dimension[6] of specimen, which is also visible in Fig.28 in Chapter 4. The first marks of crystallization of

hexagonal plates from melted phase can be found in the SEM picture of the sample heated to the temperature of 1300 °C (Fig.7), but at the temperature of 1400 °C the sample crystals do not show glassy phase. Therefore, the crystallization from non-equilibrium melt takes place.

XRD analysis of sintered sample (Fig.8) confirms the formation of non-hydraulic compound ($SrO \cdot 6Al_2O_3$) due to the reaction with bauxite. The traces of quartz in bauxite cause the formation of feldspar strontian ($SrO \cdot Al_2O_3 \cdot 2SiO_2$, described in Chapter 10.4).

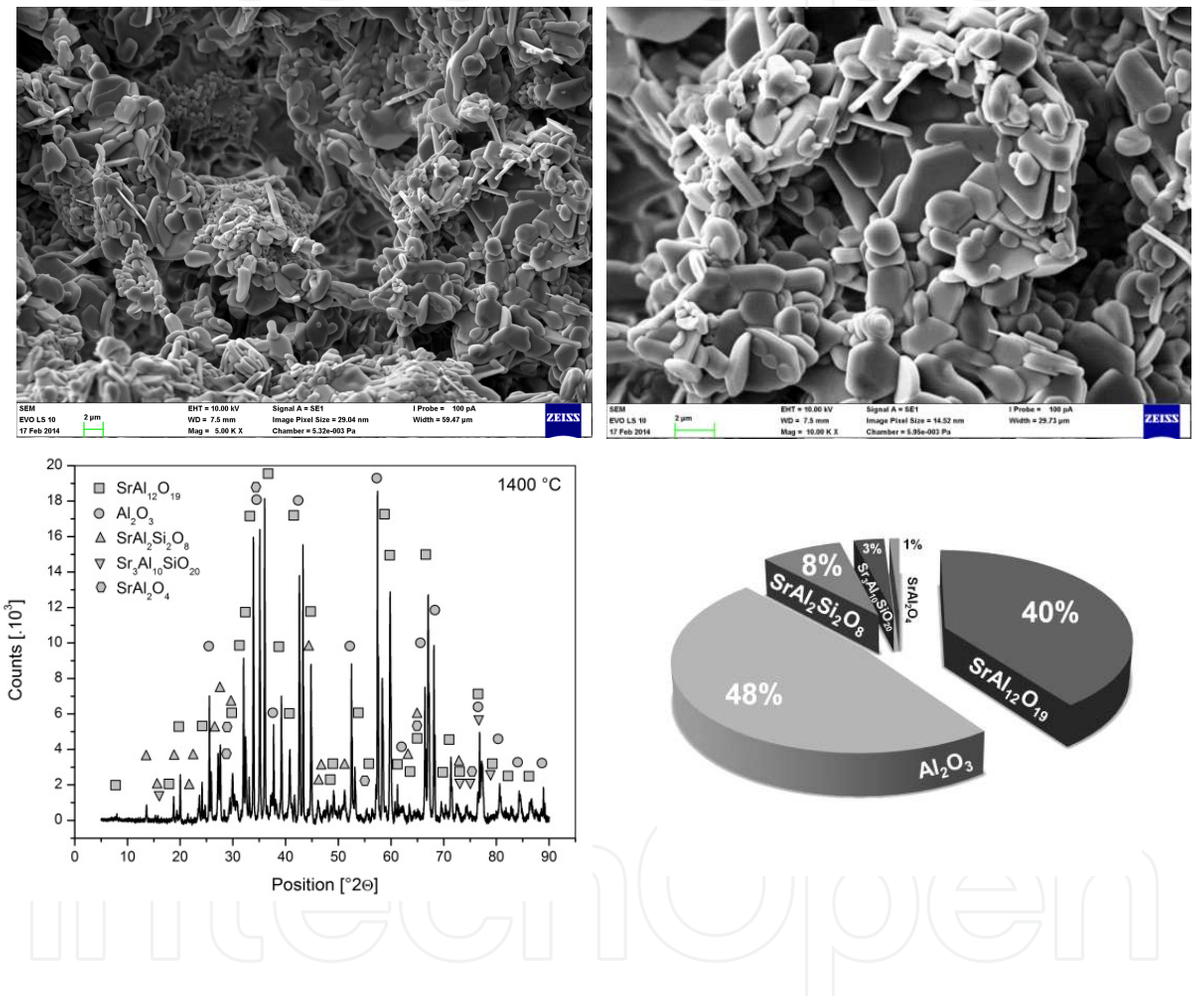


Figure 8. Electron microscopy image of refractory castable treated to the temperature of 1400°C.

Specimen heated to the temperature of 1500 °C (Fig.9) shows the volume density of 2.28 $g \cdot cm^{-3}$ and the cold crushing strength of 21.6 MPa. Measured expansion related to the thermal treatment to the temperature of 1500 °C is about 2.2 %. As the temperature increases, the small crystals are consumed during the large crystals growth and are dissolved in the melt phase.

6 This expansion should be avoided by the addition of silica bearing component into the refractory castable as was discussed in Chapter 6.2.3.

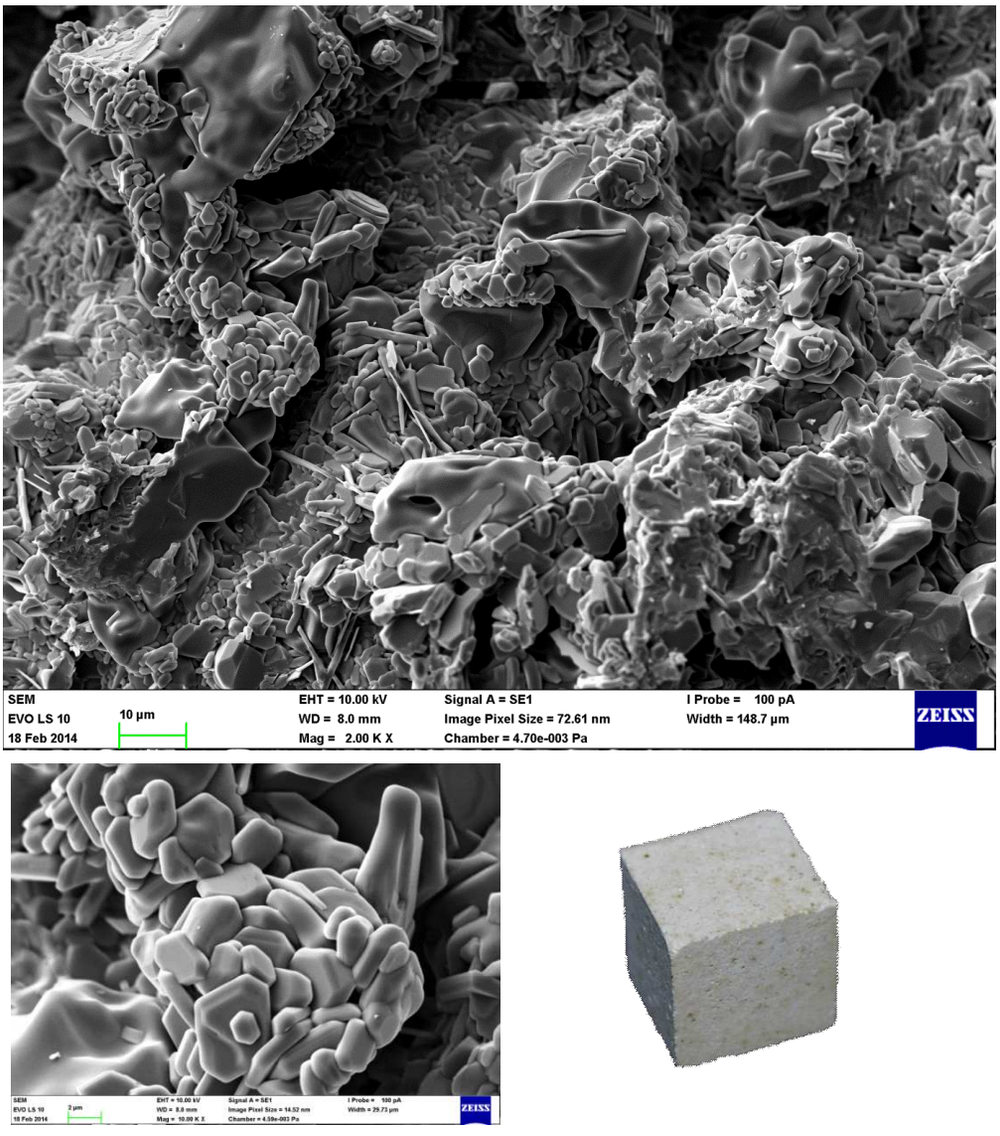


Figure 9. Electron microscopy image of refractory castable treated to the temperature of 1500°C.

After the treatment to the temperature of 1600 °C, the ceramic body of prepared refractory material consists of corundum (59 %), strontium hexaaluminate (29 %) and strontianite (12 %). Electron microscopy (Fig.10) shows that the specimen consists of large tabular pseudo-hexagonal crystals of SrA_6 surrounded by solidified glass. The sintering process reduces the dimension and porosity of the sample.

2. Insulating refractoriness

Insulating firebricks (IFBs) represent one of the refractory groups which are most commonly used for the heat insulation in industrial applications today. They are highly porous and lightweight refractories having much lower thermal conductivity and heat capacity than other

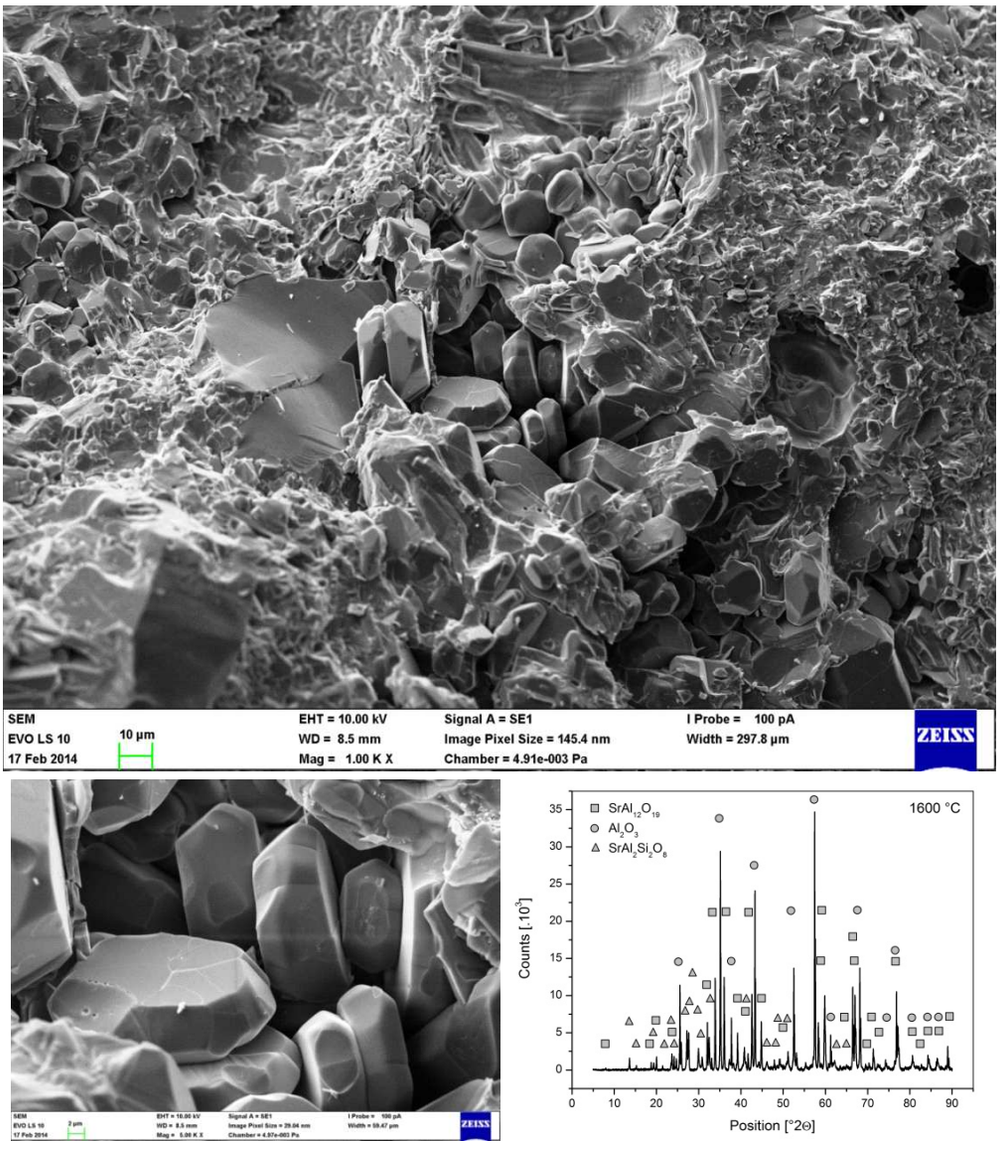


Figure 10. Electron microscopy image of refractory castable treated to the temperature of 1600°C.

refractories. Different types of insulating firebricks are manufactured mainly by using the raw materials such as diatomite, perlite, expanded vermiculite, calcium silicate, fireclay, kaolin, quartz, alumina and lightweight refractory aggregates by conventional methods. The porosity is usually created by the addition of combustible material to the raw material mixture. During firing, the combustible material burns out, and leaves large fraction of pores within the fired body [498].

Different types of pore-formers such as sawdust, foam polystyrene, fine coke, binders and organic foams, or granular materials such as hollow microspheres and bubble alumina are commonly used to obtain decreased density or to produce porous bodies in the insulating material. A considerable research is carried out recently on the reuse of pulp and paper industry wastes as a new source of raw material or pore-former in the ceramic materials due to their organic and inorganic contents [498-501].

Insulating firebricks which have highly porous structure (between 45% and 90% porosity) exhibit low thermal conductivity values. The thermal conductivity not only depends on their total porosity, but also on their pore size and shape, chemical and mineralogical composition [498]. Insulating firebricks are classified by ASTM according to the bulk density and maximum service temperature [502]. The methods for measuring the weight, dimensional measurements and bulk density of the produced bricks are defined by ASTM C134-95 [503]. Apparent porosity measurements of samples were performed by immersion into boiling water for 2 h and soaking in water for 24 h [504]. The techniques for the assessment of cold crushing strength and thermal shock resistance are specified by ASTM C133-97 [505] and ASTM C1171-96 [506], respectively.

2.1. Fillers for thermal insulating refractory castables

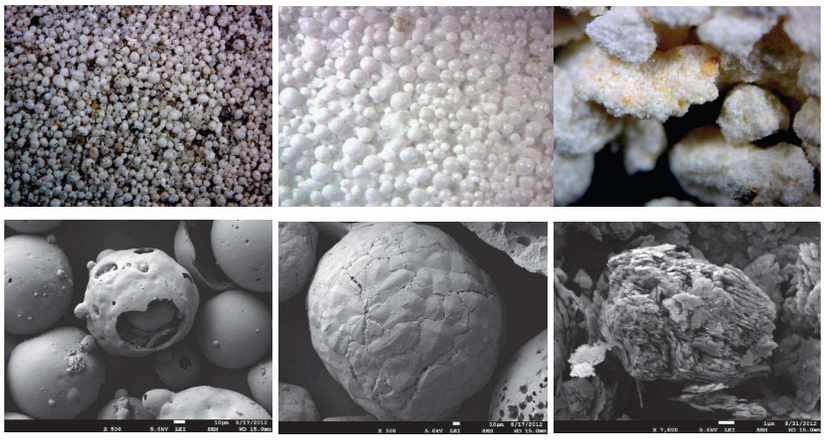


Figure 11. Examples of lightweight filler: cenospheres, bubble alumina and fireclay.

Lightweight fillers make the structure of refractory castables lighter and provide required thermal insulating properties via the formation of pores in structure. Some examples of these materials are shown in Fig.11.

2.2. Properties of refractory materials

Currently, we observe a noticeable change of climate, worldwide, probably associated with the global warming. In order to reduce the emission of greenhouse gases, especially of carbon dioxide, the generated energy should be reasonably managed. A very large amount of total energy produced in the world is heat. It is used in various industrial processes and buildings. The solution in saving the heat is a suitable construction of walls to ensure thermal insulation [507,508].

Most applications of ceramic materials are advantageously used as thermal-insulating or thermal-conducting materials. From the viewpoint of industrial applications, low thermal conductivity is needed for the thermal insulation, while high thermal conductivity is important for achieving the high heat release, high thermal shock resistance and temperature homogeneity throughout the material [509].

The quality control of thermal insulating materials typically focuses on the determination of thermal conductivity value (λ). For this purpose, special plate apparatuses are used, which are based on [510,511]:

a. Stationary heat transfer conditions;

b. Dynamic heat transfer conditions.

The heat flux vector ($\bar{q}$) is given by the Fourier´s law [509,512]:

$$\bar{q} = -\lambda \ grad \ T \quad or \quad \bar{q} = -\lambda \nabla T \tag{11}$$

$$\nabla = \left(\frac{\partial}{\partial x} \bar{i} + \frac{\partial}{\partial y} \bar{j} + \frac{\partial}{\partial x} \bar{k} \right) \tag{12}$$

where λ is the coefficient of thermal conductivity, T is the temperature. The vectors of the basis are denoted as i, j and k.

Effective thermal conductivity (ETC) is one of the key thermophysical properties used to quantify the thermal behaviour of heterogeneous materials like granular metals, ceramics, ceramic raw materials, composites, inorganic or polymeric foams, catalysts, etc. Much of the effective thermal conductivity literature is concerned with porous materials; however, the term porous itself may be the cause of a confusion. In some situations it refers to granular or particulate materials, in which the void volume may be occupied by either liquid or gaseous components; alternatively, it may refer to the material having continuous solid matrix that contains pores/bubbles, which may be isolated or interconnected. The problems may arise when a model that has been shown to work well for one type of porous material is assumed to be applicable to another type, simply because both materials are described as porous [512-514].

The Francl´s model [512,515] calculates the effective thermal conductivity of porous material (λ_e) from the thermal conductivity of solid material (λ_s) and its porosity as follows:

$$\lambda_e = \lambda_s (1 - \varepsilon) \tag{13}$$

The law was shown to be effective for a certain porous material. However, if it were applied to a granular material such as sand, the thermal conductivity would be predicted with error of several orders of magnitude.

The influence of porosity (ε) and pore size (d) on the effective thermal conductivity is described as follows [516]:

$$\lambda_e = \lambda_s (1 - \varepsilon) + \varepsilon \ \lambda_a + 4 d \sigma T^3 \tag{14}$$

where the thermal conductivity of gas phase (λ_a) and the radiation transport of heat at the temperature T are taken into account. σ denotes the Boltzmann constant.

The effective thermal conductivity of heterogeneous material is strongly affected by its composition and structure. Foams and porous materials can be considered as a two-phase (or two-component) systems consisting of solid skeleton and air, and the thermal conductivity can be described as the heat transfer through such complex system according to some of suggested analytical models [508,517-519].

Five structural models (Figs.12 and 13) are taken into account which can be expressed for two component system as follows [508,513,514,520-522,527]:

i. Series model:

$$\lambda_e = \frac{1}{(1-\nu_2)/\lambda_1 + \nu_2/\lambda_2} \tag{15}$$

ii. Parallel model:

$$\lambda_e = \lambda_1 (1-\nu_2) + \lambda_2 \nu_2 \tag{16}$$

iii. ME-1 (Maxwell-Eucken model with one continuous component) model:

$$\lambda_e = \lambda_1 \frac{2\lambda_1 + \lambda_2 - 2(\lambda_1 - \lambda_2)\nu_2}{2\lambda_1 + \lambda_2 + (\lambda_1 - \lambda_2)\nu_2} \tag{17}$$

iv. ME-2 (Maxwell-Eucken model with two continuous components) model:

$$\lambda_e = \lambda_2 \frac{2\lambda_2 + \lambda_1 - 2(\lambda_2 - \lambda_1)(1-\nu_2)}{2\lambda_2 + \lambda_1 + (\lambda_2 - \lambda_1)(1-\nu_2)} \tag{18}$$

v. EMT (Effective Medium Theory) model, which represents isotropic materials with two phases dispersed in continuous medium:

$$(1-\nu_2)\frac{\lambda_1 - \lambda_e}{\lambda_1 + 2\lambda_e} + \nu_2 \frac{\lambda_2 - \lambda_e}{\lambda_2 + 2\lambda_e} = 0 \tag{19}$$

The parameters λ and ν are the thermal conductivity and the volume fraction. The subscripts e, 1 and 2 represent two component material and its first and second constituents, respectively.

The plot of relative thermal conductivity (λ_e/λ_1) for two-component material with λ_1/λ_2=20 calculated according to the five structural models mentioned above is shown in Fig.12.

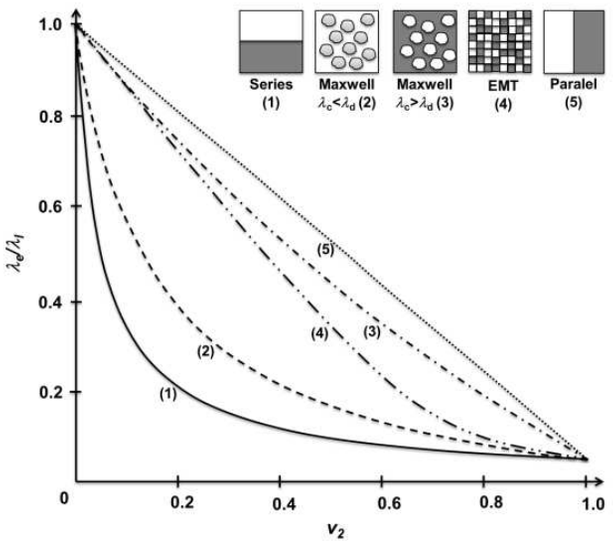


Figure 12. Relative effective thermal conductivity according to different structural models [512].

If the system consists of *i* components and is considered for *n* small spheres with the radius $\boldsymbol{R}_i$ and the thermal conductivity $\boldsymbol{\lambda}_i$, which are dispersed in uniform medium of thermal conductivity $\boldsymbol{\lambda}_m$ (Fig.13),the distribution of temperature for the single small sphere under steady-state conditions is given by the Laplace´s equation [508,512]:

$$\frac{1}{r^2}\frac{\partial}{\partial r}\left(r^2\frac{\partial T}{\partial r}\right)+\frac{1}{r^2\sin\Theta}\frac{\partial}{\partial\Theta}\left(\sin\Theta\frac{\partial T}{\partial\Theta}\right)+\frac{1}{r^2\sin^2\Theta}\frac{\partial^2 T}{\partial\varphi^2}=0 \tag{20}$$

with following boundary conditions applied:

- When $\boldsymbol{r}$=0 then $\boldsymbol{T}_i \neq \infty$.
- When $\boldsymbol{r}=\boldsymbol{R}_i$ then $\lambda_i\frac{\partial T_i}{\partial r}=\lambda_i\frac{\partial T_m}{\partial r}$ and $\frac{\partial T_i}{\partial\Theta}=\frac{\partial T_m}{\partial\Theta}$.
- When $\boldsymbol{r} >> \boldsymbol{R}_i$ then$T_m=br\cos\Theta$.

where $\boldsymbol{r}$ and $\boldsymbol{\Theta}$ are the polar radius and the polar angle, respectively, $\boldsymbol{T}$ is the temperature and $\boldsymbol{b}$ denotes the temperature gradient in the continuous medium. Assuming the symmetry of the *z*-axis so that $\boldsymbol{T}$ is independent of $\boldsymbol{\phi}$, Eq.20 has a general solution:

$$T=A+\frac{B}{r}+Cr\cos\Theta+\frac{D}{r^2}\cos\Theta \tag{21}$$

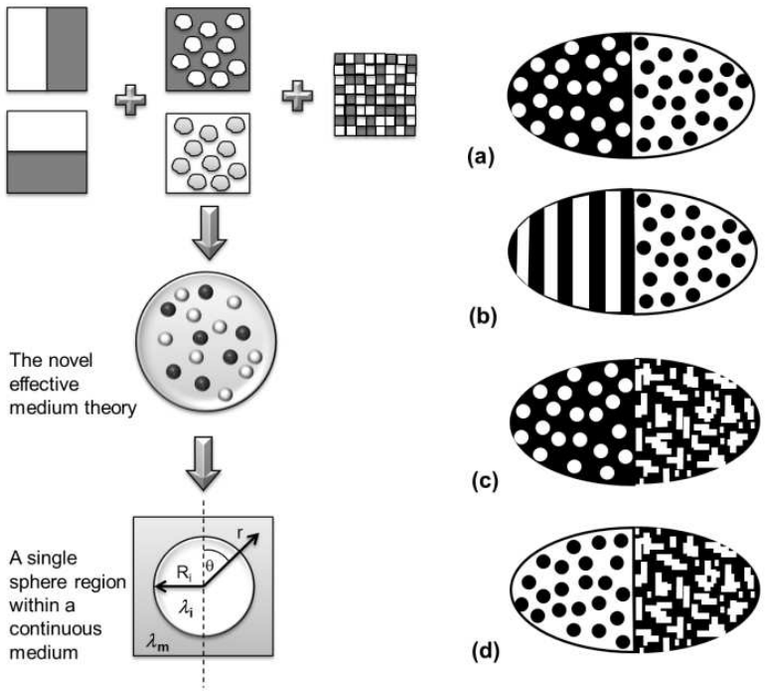


Figure 13. Structural models applied for the derivation theory for thermal conductivity of multiphase material [508] and schematic representation of tw-component material as the uniform mixture of two fundamental structural models [522]: ME-1+ME-2 (a), Parallel+ME2(b), ME-1+EMT (c) and ME-2+EMT (d).

The solution using the boundary conditions to substitute for A, B, C and D in Eq.21 and further transformation yield to the equation [508]:

$$\sum v_i \left(\frac{\lambda_i - \lambda_e}{\lambda_i + 2\lambda_m} \right) = 0 \tag{22}$$

For two-phase system (e.g. porous solid material – air) Eq.22 can be then written as:

$$(1-\varepsilon)\frac{\lambda_s - \lambda_e}{\lambda_s + 2\lambda_m} + \varepsilon \frac{\lambda_a - \lambda_e}{\lambda_a + 2\lambda_m} = 0 \tag{23}$$

where λ and ε are the thermal conductivity and the porosity and subscripts ***e***, ***a*** and ***s*** denote two-phase material, air and solid, respectively. Eq.23 represents individual structural models:

- Series model when λ_m=0;
- Parallel model when λ_m=∞;
- Maxwell-Eucken model with one continuous component when λ_m=λ_s;
- Maxwell-Eucken model with two continuous components when λ_m=λ_a;

- EMT model when $\boldsymbol{\lambda}_{\mathrm{m}}=\boldsymbol{\lambda}_{\mathrm{e}}$.

To avoid potential misapplication of the effective thermal conductivity models, the materials which may be described as porous should be divided into two classes:

1. Internal porosity materials which have bubbles/pores suspended within a continuous condensed phase (e.g. sponges, foams, honeycombs), where the optimal heat transfer pathway is through the continuous phase.
2. External porosity materials which include granular particulate materials where the optimal heat conduction pathway is through the dispersed phase.

A model that accurately predicts the effective thermal conductivity of internal porosity materials will not necessarily be applicable to external porosity materials or vice versa.

Carson at al. [512] proposed that the effective thermal conductivity of internal porosity materials was bounded above by the Maxwell–Eucken equation for the lower-conductivity material as the dispersed phase, and below by the EMT equation; and that the effective thermal conductivity of external porosity materials is bounded above by the EMT equation, and below by the Maxwell–Eucken equation for the lower conductivity material as the continuous phase.

The equation which unifies five structural models mentioned above for heterogeneous material was developed by Wang [522]:

$$\lambda_e = \frac{\sum_{\mathrm{i}=1}^{\mathrm{m}} \lambda_{\mathrm{i}} v_i \frac{d_i \bar{\lambda}}{(d_i - 1)\,\bar{\lambda} + \lambda_i}}{\sum_{\mathrm{i}=1}^{\mathrm{m}} v_i \frac{d_i \bar{\lambda}}{(d_i - 1)\,\bar{\lambda} + \lambda_i}} \tag{24}$$

Each structural model can be derived by suitable choice of parameters $\boldsymbol{d}_{\mathrm{i}}$ and $\bar{\lambda}$:

- Series model when $d_i=1$ or $\bar{\lambda} \to 0$;
- Parallel model when $d_i=\infty$ or $\bar{\lambda} \to \lambda_i$;
- Maxwell-Eucken model when $d_i=3$ or $\bar{\lambda} \to \lambda_m$;
- EMT model when$d_i=3$ or $\bar{\lambda} \to \lambda_e$.

Parameter $\boldsymbol{d}_{\mathrm{i}}$ can have a physical interpretation. Kirkpatrick [523] related similar parameter to the number of Euclidean dimensions of the system involved, while Fricke [524] and Hamilton and Crosser [525] related it to the sphericity of dispersed phase. However, it may be possible to define a parameter that combines both aspects; the component shape and the number of Euclidean dimensions. This is the topic of ongoing investigations by the authors, but it falls outside the scope of this publication. The most common approach is to use $\boldsymbol{d}_{\mathrm{i}}=3$ (spherical dispersed phase) [508,522].

The model suggested by Levy [526] is based on the Maxwell–Eucken model and is based solely on algebraic operations and has no stated physical basis:

$$\lambda_e = \lambda_1 \frac{2\lambda_1 + \lambda_2 - 2(\lambda_1 - \lambda_2)F}{2\lambda_1 + \lambda_2 + (\lambda_1 - \lambda_2)F} \tag{25}$$

where

$$F = \frac{2/G - 1 + 2\nu_2 - \sqrt{(2/G - 1 + 2\nu_2)^2 - 8\nu_2/G}}{2} \tag{26}$$

$$G = \frac{(\lambda_1 - \lambda_2)^2}{(\lambda_1 + \lambda_2)^2 + \lambda_1\lambda_2/2} \tag{27}$$

In order to make the basic structural models more general for different structures, the additional parameter is sometimes introduced. The Krischer's approach assumed that the complex structure could be approximated by a mixture of simpler structures, where the relative amounts of each of the simpler structures was determined empirically. We define the ''structure volume fractions (ε_j)'' to be distinct from the component volume fractions (ν_i) for the ***j***-th type of structure by the relation [522]:

$$\varepsilon_j = \sum_i \nu_i \phi_{ij} \tag{28}$$

$$\sum_j \varepsilon_j = 1 \tag{29}$$

The ''structure composition factors'' ϕ_{ij}, are the measures of the fractions of material component *i* that is a part of structure *j*. Therefore the total amount of component i must be distributed between the structures:

$$\sum_j \phi_{ij} = 1 \tag{30}$$

The effective thermal conductivity of structureΛ_j, which consists of *n* components, is the function:

$$\Lambda_j = \Lambda_j(\nu_1, \nu_2 \ldots \nu_n, \phi_{1j}, \phi_{2j} \ldots \phi_{nj}, \lambda_1, \lambda_2 \ldots \lambda_m) \tag{31}$$

Since this structure can be described by one of five structural models listed above, it can be written as[7]:

$$\Lambda_j = \frac{\sum_{i=1}^{m} \lambda_i \nu_i \phi_{ij} \dfrac{d_i \bar{\lambda}}{(d_i - 1)\,\bar{\lambda} + \lambda_i}}{\sum_{i=1}^{m} \nu_i \phi_{ij} \dfrac{d_i \bar{\lambda}}{(d_i - 1)\,\bar{\lambda} + \lambda_i}} \tag{32}$$

The effective thermal conductivity of the material which is formed from z structures can be considered for the function:

$$\lambda_e = \lambda_e(\Lambda_1, \Lambda_2 \cdots \Lambda_z) \tag{33}$$

In order to solve Eq.32, based only on λ_i and ν_i without any empirical parameters, it is necessary to determine the expressions for ϕ_{ij} as functions of λ_i and ν_i. Therefore, the assumption of relative amounts of each structure ε_j, in total volume and of relative contributions of different Λ_j to λ_e is necessary. The infinite number of relationships between ε'_j and Λ_j could be found. It is possible to relate ε'_j to structural characteristics. However, such detailed information is often unavailable. Therefore the simplest possible relationships were adopted. They are to assume that each structure comprises an equal fraction of total volume:

$$\varepsilon_j = \frac{1}{z} \tag{34}$$

and that the thermal conductivity of each structure is equal to the effective thermal conductivity:

$$\lambda_e = \Lambda_1 = \Lambda_2 = \cdots = \Lambda_z \tag{35}$$

The solution for selected binary structure models (Fig.13) with suitable choice of d_i and $\bar{\lambda}$ according to Eq.24 can be expressed as follows [522]:

1. ME-1+ME-2 model:

$$\lambda_e = \frac{\lambda_1 \nu_1 \phi_{11} + \lambda_2 \nu_2 \left(\dfrac{1 - 2\nu_1 \phi_{11}}{2\lambda_2}\right)\left(\dfrac{3\lambda_1}{2\lambda_1 + \lambda_2}\right)}{\nu_1 \phi_{11} + \nu_2 \left(\dfrac{1 - 2\nu_1 \phi_{11}}{2\lambda_2}\right)\left(\dfrac{3\lambda_1}{2\lambda_1 + \lambda_2}\right)} \tag{36}$$

7 Please consult with Eq.24.

2. Parallel+ME-2 model:

$$\lambda_e = \frac{\lambda_1 \nu_1 \phi_{11} + \lambda_2 \nu_2 \phi_{21}}{\nu_1 \phi_{11} + \nu_2 \phi_{21}} = \frac{\lambda_2 \nu_2 \phi_{22} + \lambda_1 \nu_1 \phi_{12} \dfrac{3\lambda_2}{2\lambda_2 + \lambda_1}}{\nu_2 \phi_{22} + \nu_1 \phi_{12} \dfrac{3\lambda_2}{2\lambda_2 + \lambda_1}} \tag{37}$$

3. ME-1+EMT model:

$$\lambda_e = \frac{C + \sqrt{C^2 + 2\lambda_1 \lambda_2}}{2} \tag{38}$$

where

$$C = (2\lambda_1 - \lambda_2)\nu_1 \left(\frac{2\nu_1 + 2\nu_2 \phi_{21} - 1}{2\nu_1} \right) + (2\lambda_2 - \lambda_1)\nu_2 (1 - \phi_{21}) \tag{39}$$

4. ME-2+EMT model:

$$\lambda_e = \frac{D + \sqrt{D^2 + 2\lambda_1 \lambda_2}}{2} \tag{40}$$

where

$$D = (2\lambda_1 - \lambda_2)\nu_1 (1 - \phi_{11}) + (2\lambda_2 - \lambda_1)\nu_2 \left(\frac{2\nu_2 + 2\nu_1 \phi_{11} - 1}{2\nu_2} \right) \tag{41}$$

For ternary-structure models composed of EMT+ME-2+Series the following can be derived [522]:

$$\lambda_e = \frac{\lambda_1 \nu_1 \phi_{12} \dfrac{3K}{2K + \lambda_1} + \lambda_2 \nu_2 \phi_{22} \dfrac{3K}{2K + \lambda_2}}{\nu_1 \phi_{12} \dfrac{3K}{2K + \lambda_1} + \nu_2 \phi_{22} \dfrac{3K}{2K + \lambda_2}} \tag{42}$$

Where:

$$\nu_1\phi_{11} + \nu_2\phi_{21} = 1/3$$
$$\nu_1\phi_{12} + \nu_2\phi_{22} = 1/3$$
$$\nu_1\phi_{13} + \nu_2\phi_{23} = 1/3$$
$$\phi_{11} + \phi_{12} + \phi_{13} = 1$$
$$\phi_{21} + \phi_{22} + \phi_{23} = 1$$

Krischer uses the empirical approach *f* which is sometimes referred as the distribution factor. This parameter ranges from 0 to 1 and serves as the weighting factor that makes the basic structural model more universal for different structures. The value of this parameter must be determined by the experiment. This parameter is used in [508,522,527]:

- **Krischer model**, i.e. weighted harmonic mean between the series model and the parallel model:

$$\lambda_e = \frac{1}{\frac{1-f}{\lambda_1(1-\nu_2)+\lambda_2\nu_2} + f\left(\frac{1-\nu_2}{\lambda_1}+\frac{\nu_2}{\lambda_2}\right)} \tag{43}$$

- **Hamilton model:**

$$\lambda_e = \lambda_1 \frac{(f-1)\lambda_1 + \lambda_2 - (f-1)(\lambda_1-\lambda_2)\nu_2}{(f-1)\lambda_1 + \lambda_2 + (\lambda_1-\lambda_2)\nu_2} \tag{44}$$

- **Chaudhary-Bhandari model:**

$$\lambda_e = \left[\lambda_1(1-\nu_2)+\lambda_2\nu_2\right]^f \left(\frac{1-\nu_2}{\lambda_1}+\frac{\nu_2}{\lambda_2}\right)^{(1-f)} \tag{45}$$

- **Kirkpatrick model:**

$$\sum_{i=1}\nu_i \frac{\lambda_i - \lambda_e}{\lambda_i + \left(f/2 - 1\right)\lambda_e} = 0 \tag{46}$$

2.3. Thermal insulating castables

The refractory castables filled by cenospheres (Fig.14), alumina bubbles (Fig.15) and fireclay (Fig.16) were prepared as an example of thermal insulating castables based on strontium aluminate cement. The specimens were prepared using strontium aluminate cement, bauxite and filler in the mass ratio of 1:3:1 and ***w/c***=1. The applied opening material was described in Chapter 6.1.3.

The microphotographs and some properties and information on applied filler can be found in Chapter 6.2.1.

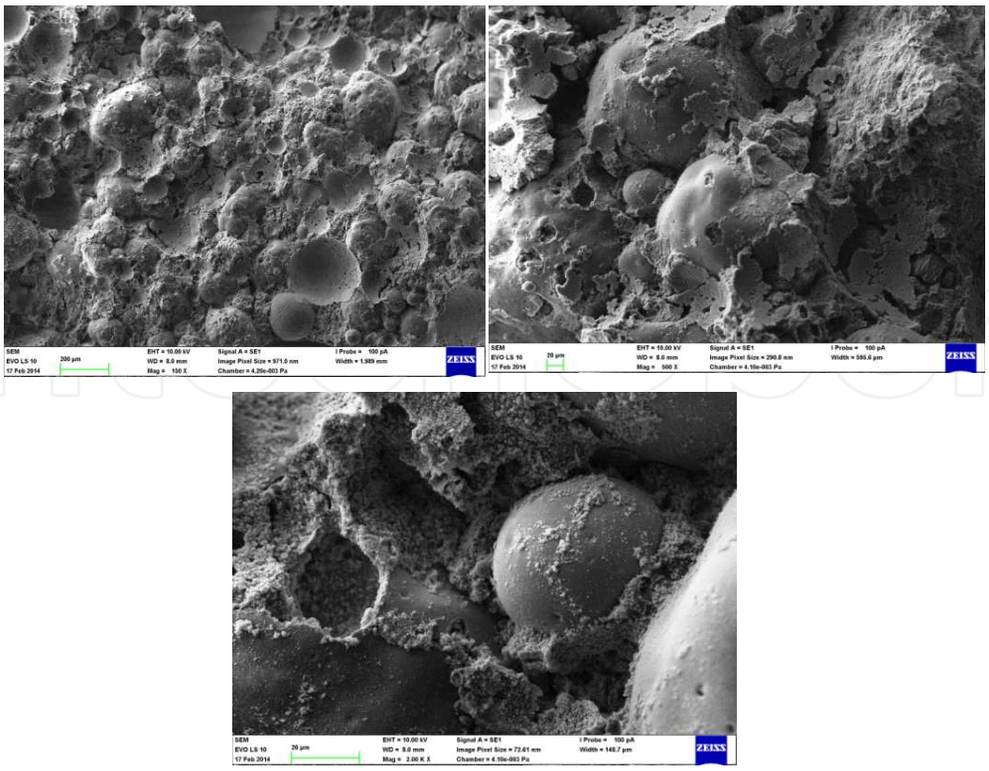


Figure 14. Thermal insulating castable based on cenospheres.

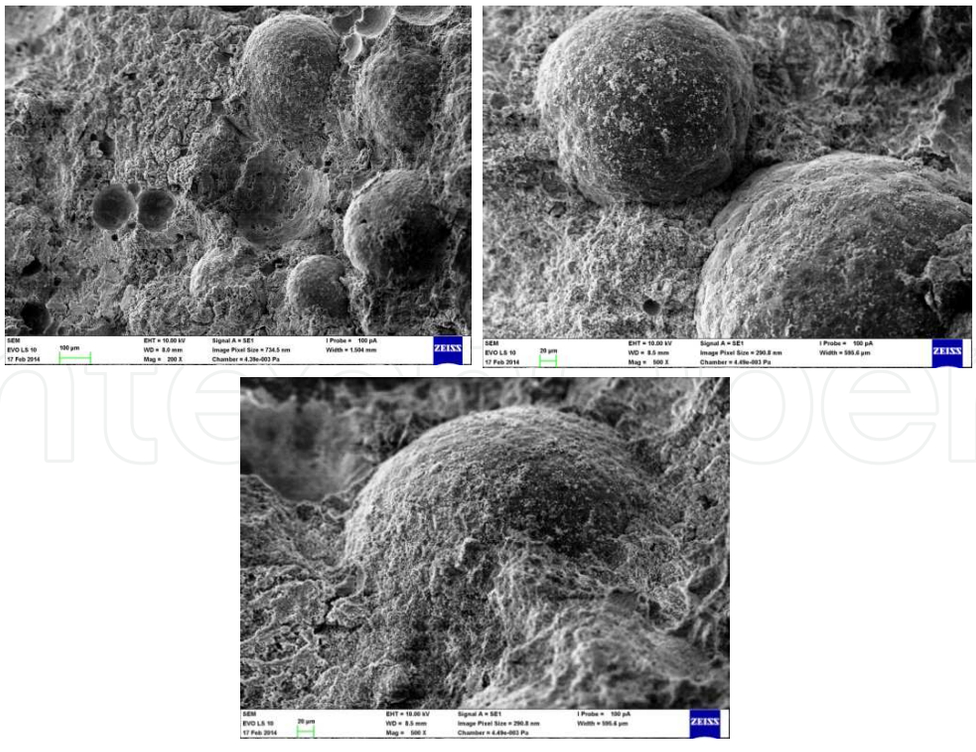


Figure 15. Thermal insulating castable filled with alumina bubbles.

Some properties of prepared samples of thermal insulating castables before and after (Fig. 17) thermal treatment are listed in Table 3.

Used opening material	Volume density [g.cm^{-3}]		Shrinkage [%]			Cold crushing strength [MPa]
	After setting	After thermal treatment	Autogenous	Thermal treatment	Total	
Cenosphere	1.28	1.65	0.3	25.0	25.3	---
Bubble alumina	2.05	1.76	0.3	+6.3*	+6.6*	16.2
Fireclay	1.96	2.25	+4.0*	11.4	15.4	24.7

* Expansion with regard to the initial volume of specimen.

Table 3. Properties of thermal insulating castable before and after thermal treatment to 1500°C.

While the dimensions of thermal insulating castables prepared with cenospheres and fireclay were reduced, the expansion was observed for the sample prepared with bubble alumina filler (Table 3).

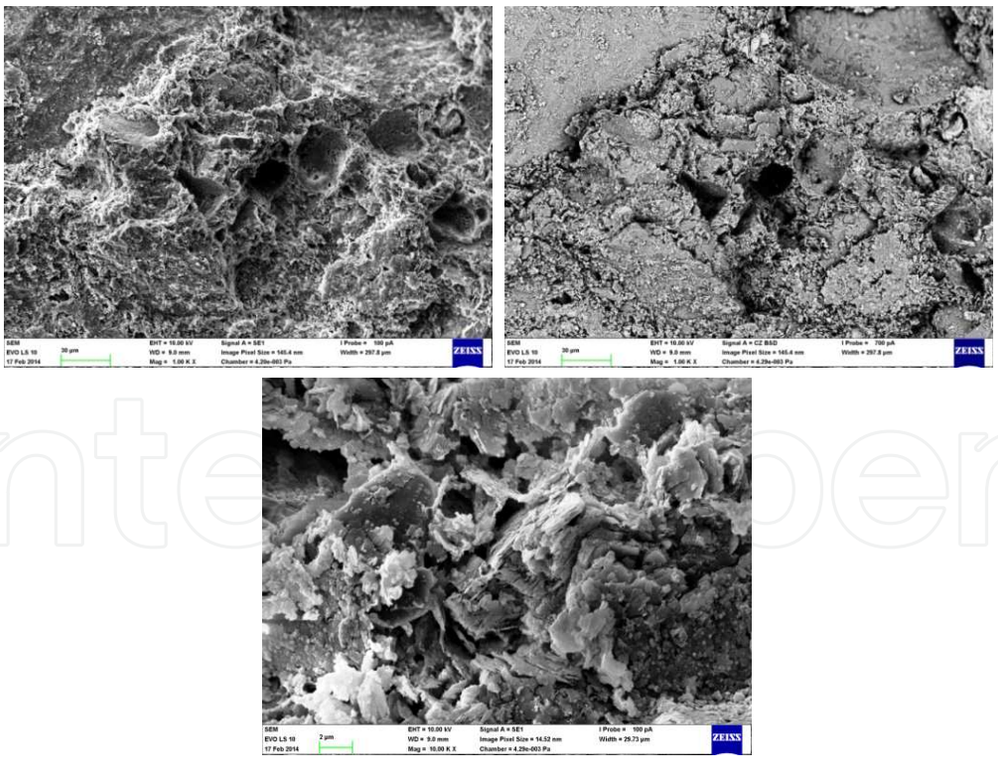


Figure 16. Thermal insulating refractory castable prepared with fireclay.

The reason for the expansion behaviour of this sample is probably the same as for dense refractory castables filled by bauxite (Chapter 6.1.5). Observed behaviour provides some really

interesting possibilities to control the volume changes during the thermal treatment. Since the addition of alumina led to the expansion (recrystallization) and the addition of fireclay to the shrinkage (formation of SrO Al_2O_3 $2SiO_2$ and sintration), the proper mutual ratio of these constituents enables to prepare the dimension stable refractory.

Furthermore, the addition of fireclay enables to avoid undesirable growth of large crystals during the thermal treatment (please compare Figs.7-10). The introduction of cenospheres led to the formation of eutectic melt with iron, therefore they are not optimal for high temperatures and reductive conditions.

X-ray diffraction analysis of samples prepared with fireclay and cenospheres confirms the formation of strontianite and strontium hexaaluminate (SrA_6) in the ceramic body (Fig.17(b)). Due to missing source of SiO_2, strontianite isn't formed in the sample prepared with bubble alumina. Corundum is the main phase in all prepared samples.

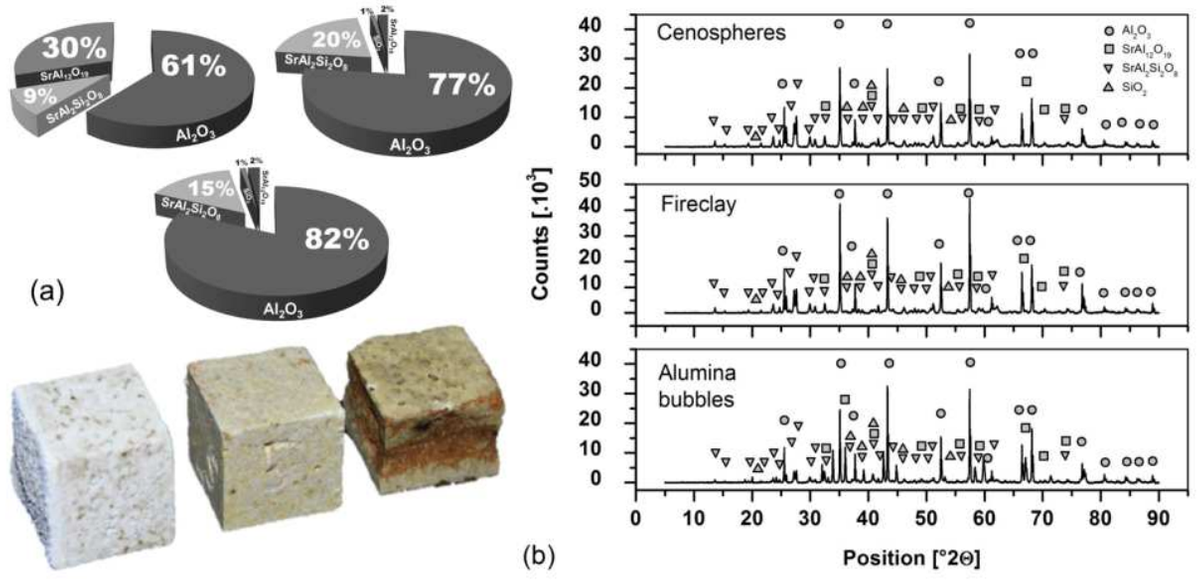


Figure 17. Specimens prepared with bubble alumina, fireclay and cenospheres treated to the temperature of 1500 °C (a) and x-ray diffraction analysis of prepared samples (b).

The microphotographs of fracture area of thermal insulating refractory castable filled with alumina bubbles after the thermal treatment is shown in Fig.18. The bubbles are surrounded by hexagonal crystals of recrystallized strontium aluminate matrix of binding phase. The inner side of alumina balls shows well-developed crystals of alumina.

Thermal insulating castable prepared with fireclay and fired to the temperature of 1500 °C is shown in Fig.19. The specimen texture shows large bauxite grains covered by matrix of recrystallized strontium aluminate phase where the artefacts of layered aggregate of fireclay filler can be seen.

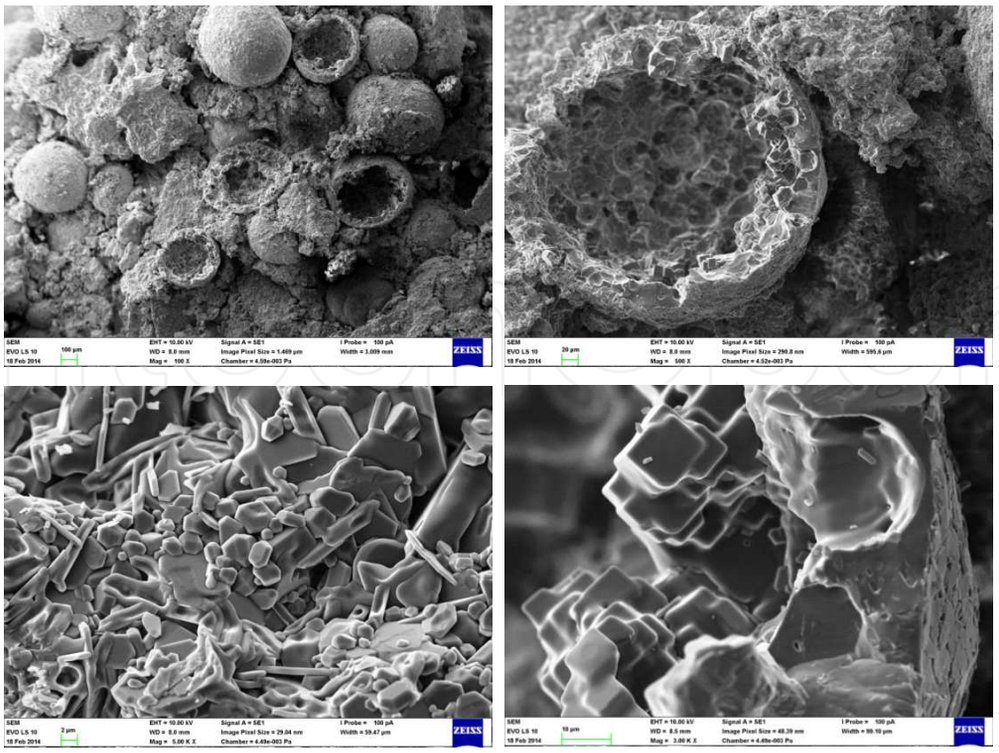


Figure 18. Thermal insulating refractory castables with bubble alumina treated to the temperature of 1500 °C.

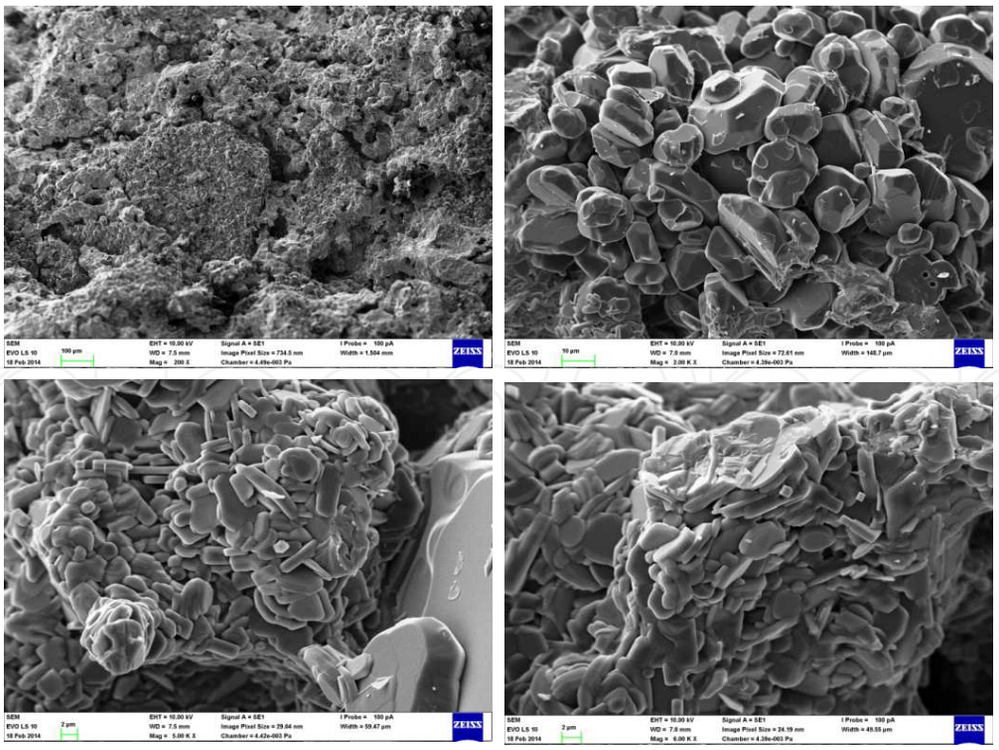


Figure 19. Thermal insulating refractory castables with fireclay treated to the temperature of 1500 °C.

Large amount of melt phase formed during the thermal treatment of specimen prepared with cenospheres led to extensive sintering, firing shrinkage and deformation of the shape. Cenospheres were completely dissolved in formed eutectic melt and there is no artefact in the body of specimen after the thermal treatment. The SEM analysis (Fig.20) shows the strontium aluminate crystals surrounded by glassy phase.

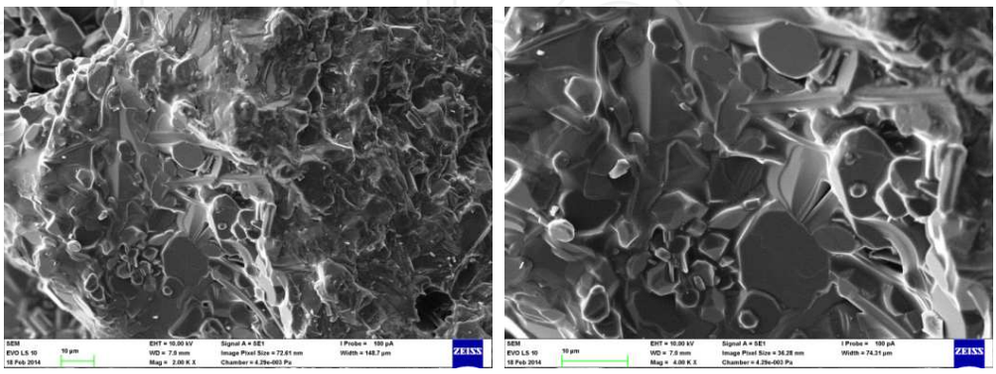


Figure 20. Thermal insulating refractory castables with cenospheres treated to the temperature of 1500 °C.

3. Ceramic Foams

3.1. Properties and processing of ceramic foams

Foams can be defined as dispersion systems based on the bubble gas phase, usually air, in continuous matrix of liquids-"aqueous and non-aqueous liquid foams", or solids "solid foams" (e.g. pumice as well as steel, glass and concrete foams). The diameter of bubbles is usually of several millimeters, but the spherical shape is not common as the weight of foam leads to mutual deformation and to the formation of irregular polyhedral cells. The structure of foams is often compared to honeycombs. The walls of bubbles make always the same angle of 120° hence maximum four bubbles can be in contact at one point. This structure provides foams with certain mechanical strength and elasticity [528-531].

Liquid foams are usually prepared via mechanical dispersion of gas in liquid in the presence of surfactants. These compounds reduce the surface tension via the formation of films on the interface as they contain both the hydrophobic and the hydrophilic groups. Foams are then always formed under dynamic conditions so the adsorption equilibrium of surfactant is usually not achieved. Applied kind and concentration of surfactant determine the time-stability and the structure of foams. Higher viscosity of surface layer, its flexibility and hydration of polar groups of surfactant decelerate the water flow-out from bubble walls and thus are the factors contributing to the time-stability of foams. This fact may have a significant effect on the magnitude of forces stabilizing the foam and foam films [530,532-536].

The research on the structure, behaviour and properties of foams is motivated by both, the preparation of foams and the prevention from undesirable formation of foam. For technical

applications (usually filters, carriers of catalysts, biomaterials, thermal insulating materials, refractories [531,537,538]) the factors such as the stability, specific surface and porosity of foams are important. Foams were also used in wide range of industrial processes e.g. flotation [539].

As for the time-stability of foams, the control of bubble size and the preparation of monodispersed foams are intensively studied [540]. The structure and the processes of coarsening and drainage of foams [541] and their dynamics are also affected by fine particles [542-546].

Open cell (reticulated) ceramic foams, which are defined as dispersion systems based on the interconnected bubbles of gas phase in continuous ceramic matrix, can be prepared via different manufacturing techniques [531,547] including the transformation of ceramic powder slurry into the solid foam [536,548,549], the reticulated sponge method (replica technique) [550-553], the gel casting [554-557], the bubble generation methods [558] or direct foaming [559]. The replica technique is based on the pyrolysis of a polymeric sponge coated by ceramic slurry. Following high-temperature treatment leads to the ceramic bond via sintering. The gel casting method uses the mechanical work and foaming agents in order to foam the ceramic suspension.

Cellular cement is a lightweight material consisting of Portland cement (PC) [560,561], alumina cement (AC) [562,563] or blended cements [564,565] paste or mortar with homogeneous void or cell structure created by introducing air or gas in the form of small bubbles. Cement and concrete foams can be made by adding aluminium powder to the mix before adding gauging water or by injecting aqueous foaming agent to the cement slurry to give foams with the porosity of 50-90 %. Microsilica and a plasticizer were added to the cement-water slurry and polyester fibers were incorporated to improve the foam stability and strength [566-569]. Foamed concrete was patented in 1923 [570,571].

Using mixed cationic/anionic surfactants in aqueous foam systems has been of an interest for several years because they could provide good foam stability [572].Therefore the mixed surfactants used in pure aqueous foams are intensively studied [535,536,573].

In order to evaluate the maximum capillary pressure ($\boldsymbol{P}_{C,max}$ [MPa]) and the effective bubble pressure for a stable bubble ($\Delta\boldsymbol{P}_{eff}$ [MPa]), the following relationships can be used [543,574,575]:

$$P_{C,\max} = \frac{4 f \gamma}{R_P}\left(\cos\Theta + Z\right) \tag{47}$$

and

$$\Delta P_{eff} = \left(P_{atm} + \frac{2\gamma}{R_B} + \rho g H\right)\left[1 - f\left(1 - \cos^2\Theta\right)\right] \tag{48}$$

where f is the fraction area of the bubble's surface that is coated by particles, Θ is the wetting angle of particles [°], R_P is the particle's radius [m], γ is the surface tension [N m^{-1}] on the gas-liquid interface and Z is a parameter related to the sort of particle configuration within the

film, P_{atm} is the atmospheric pressure [0.101 MPa], ρ is the foam density [kg m^{-3}], $\boldsymbol{g}$ is the gravity acceleration [m s^{-2}], $\boldsymbol{H}$ is the height of foam column [m] and $2\boldsymbol{R}_B$ is the bubble diameter. The term $\rho\boldsymbol{gH}$ is also known as the hydraulic pressure. The Laplace pressure due to the radius of curvature of the bubble is considered in the term of $2\gamma/\boldsymbol{R}_B$. The value of $\Delta\boldsymbol{P}_{C,max}$ is not the function of bubble size and Eq.48 is not a function of the particles size at the bubble's film.

The approach for the calculation of foam "**stability index**" (***SI***) proposed by Vivaldini et al. [575] in order to combine the $\boldsymbol{P}_{C,max} - \Delta\boldsymbol{P}_{eff}$ difference with $\Delta G_{ads}/\boldsymbol{k}_B\boldsymbol{T}$ ratio is given by the following equation:

$$SI = \left(P_{C,\max} - \Delta P_{eff}\right)\frac{\Delta G_{ads}}{k_B T} \tag{49}$$

where $\Delta\boldsymbol{G}_{ads}$ is the adsorption free energy [J] of the particles at the bubble interface regarding their thermal energy expressed by term $\boldsymbol{k}_B\boldsymbol{T}$ [J]. The symbols $\boldsymbol{k}_B$ and $\boldsymbol{T}$ denote the Boltzmann constant and the temperature, respectively. The dimension-less ratio $\Delta G_{ads}/\boldsymbol{k}_B\boldsymbol{T}$ (adsorption energy/ thermal energy) then describes the stability of the gas-liquid interface.

When a particle is attached to a gas-liquid interface, the overall Gibbs free energy of the system is reduced, which makes this process thermodynamically favorable. The energy decrease due to this adsorption process at a flat interface can be for $0 \le \boldsymbol{\Theta} \le 90°$ mathematically described by the equation:

$$\Delta G_{ads} = \pi\, R_P^2\, \gamma\left(1 - \cos\Theta\right)^2 \tag{50}$$

Nevertheless, the $\Delta\boldsymbol{G}_{ads}$ value cannot be used to state whether the interface is stable or not. That argument can only be sustained when the energy released due to the adsorption of particles is compared to their own thermal energy, which is the origin of the Brownian motion of colloidal particles in suspension [575,576].

3.2. Ceramic foams stabilized by HAC

Since water is consumed by hydration, calcium aluminate cement can be used for the stabilization of raw ceramic foams. Moreover, setting of cement confers the mechanical properties to foam, which enable the manipulation prior to drying and thermal treatment. Some examples of foamed materials prepared using the techniques described in works [577,578] are shown in Fig.21. The ceramic bond formed during the thermal treatment enables to cut tapes or desks by cutting and shaping the original foamed large cast profile.

Large aggregates of kaolinite particles are delaminated and redistributed closer to the surface of liquid phase to form the solid framework of foam. The thickness of the bubble walls is approximately ten times smaller than the median of particle size of applied kaolinite. Foam with the thickness of walls of 100 nm can be prepared. Hence forced delamination of kaolinite aggregates occurs and the lamellar particles of kaolinite form the framework or solid replica

of original liquid bubble wall. The thermal treatment of foam provides the ceramic foam of high service temperature and chemical stability, with high specific surface area, extremely low volume density and excellent thermal insulating properties [577,579].



Figure 21. Examples of refractory foam prepared with calcium aluminate cement (a). Raw and fired block of ceramic foam (b).

3.3. Ceramic foams stabilized by SrAC

Since the ceramic foam can be stabilized by calcium aluminate cement, it is possible to use also strontium aluminate cement for the same purpose. On the other hand, there are some differences in hydration and setting of both cements as was discussed in Chapter 5. The application of additives or certain modification of foam processing is necessary in order to improve the cement behaviour (Chapter 5.4).

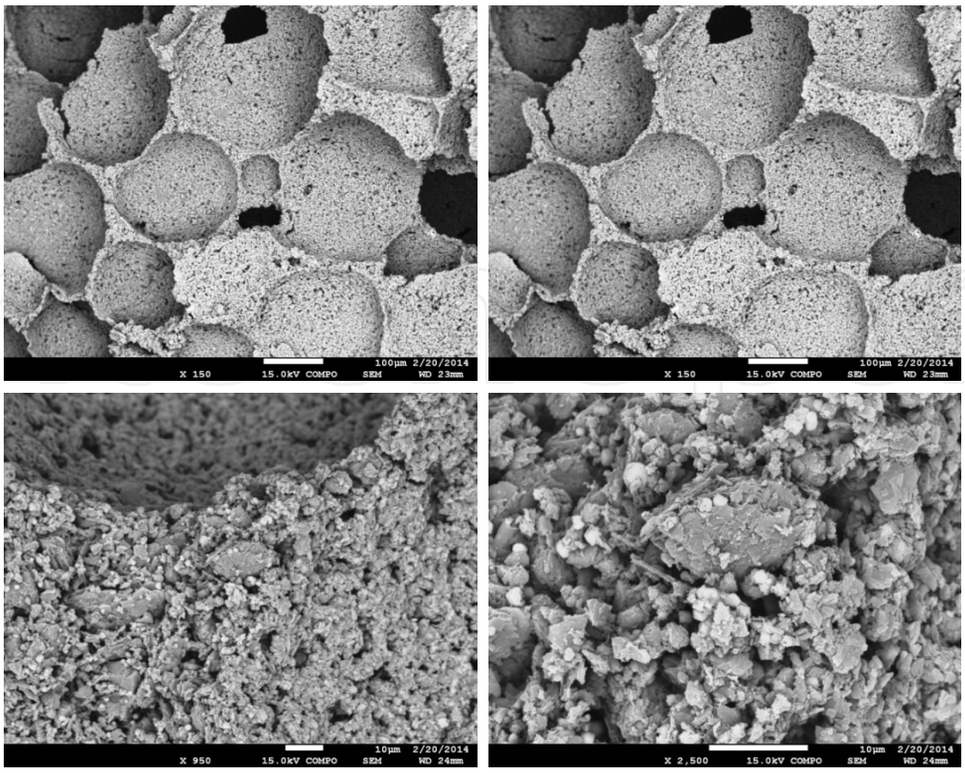


Figure 22. Raw foam before the thermal treatment.

The microphotograph of raw foam prepared via foaming the slurry prepared from strontium aluminate cement, meta-kaolinite and water in the mass ratio of 1:4:5 is shown in Fig.22. Applied method is analogical to the techniques used for the preparation of foam with calcium aluminate cement [577,578], but formed structure is quite different from the foam prepared with kaolinite. The reorganization of particles from original aggregates of kaolinite does not occur in metakaolinite. That results in the formation of thick-walled cells with more spherical shape.

The morphology of foam cells before and after the thermal treatment shows that the walls of cells in foam form an angle of ~120°. The microphotograph of foam treated to the temperature of 1500 °C is shown in Fig.23. The SEM picture shows sintered foam, where the side walls of bubbles contain large amount of needle-like crystals of mullite.

The results of thermal analysis (Fig.24(a)) show that drying, the thermal decomposition of hydrates and the pyrolysis of surfactant takes place up to the temperature of 300 °C. Large surface of foamed structure supports the carbonation. Therefore the content of carbonates in foamed samples is usually higher than that in dense materials. The thermal decomposition of $SrCO_3$ and removing of residual water from metakaolinite leads to the decrease of the sample mas by 3.4 % within the temperature range from 550 to 900 °C. SrO formed during the thermal decomposition of strontium carbonate is a reactive species which reacts with both, metakaolinite and other strontium aluminates, to strontium aluminate and Sr-gehlenite (strontiogehlenite, $SrAl_2SiO_7$ [580,581]).

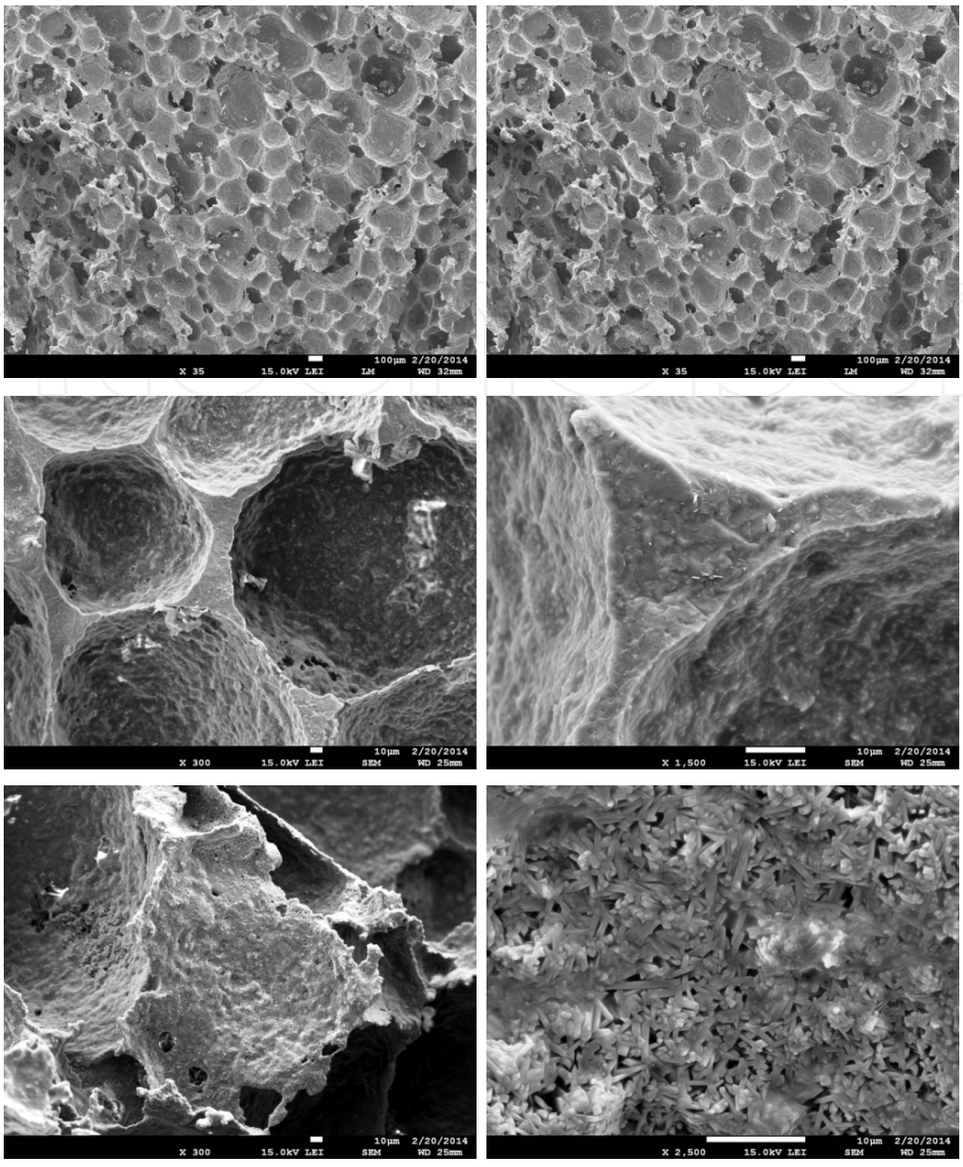


Figure 23. Foam after the thermal treatment to 1500 °C.

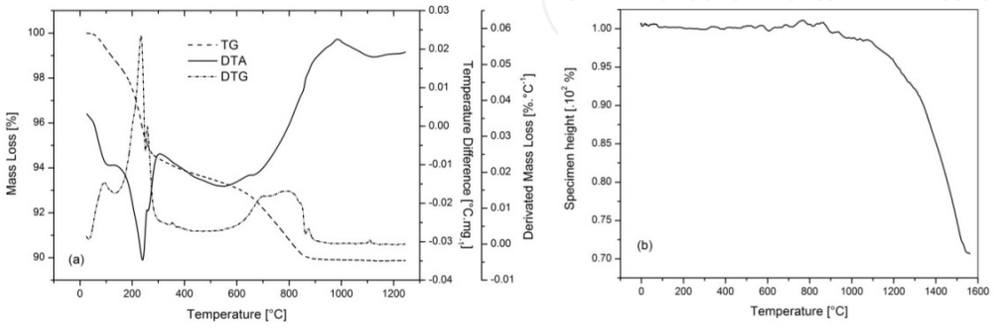


Figure 24. TG-DTA (a) and heating microscopy (b) of raw foam.

The abundance of metakaolinite leads to the formation of usual and well described products such as Al-Si spinel phase and mullite [582,583]. Strontium bearing aluminosilicates are further transformed to Sr-celsian with increasing temperature [584-586,893]. The temperature, which is required for the preparation of sintered sample was determined by heating microscopy (Fig. 24(b) and Fig.25). The sintering begins at the temperature of 1350 °C.

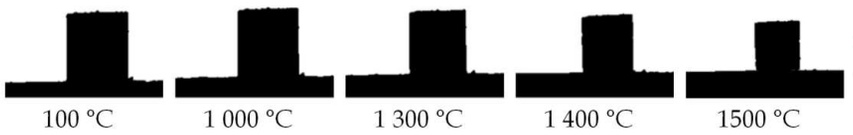


Figure 25. The behaviour of specimen of foam during heating to the temperature of 1550 °C at the rate of 5 °C min^{-1}.

Infrared spectrum of foam before the thermal treatment (Fig.26(a)) shows the features of meta-kaolinite [587], strontium carbonate, hydrogarnet, gibbsite, surfactant (C-H stretching in -CH_3 and -CH_2 groups in the region from 2975 to 2825 cm^{-1}) as well as the stretching (3440 cm^{-1}) and bending bands (1460 cm^{-1}) of absorbed water. The spectral features of $SrCO_3$, gibbsite and Sr_3AH_6 were already described in Chapter 5.1. Excessive carbonation results from high surface of foam.

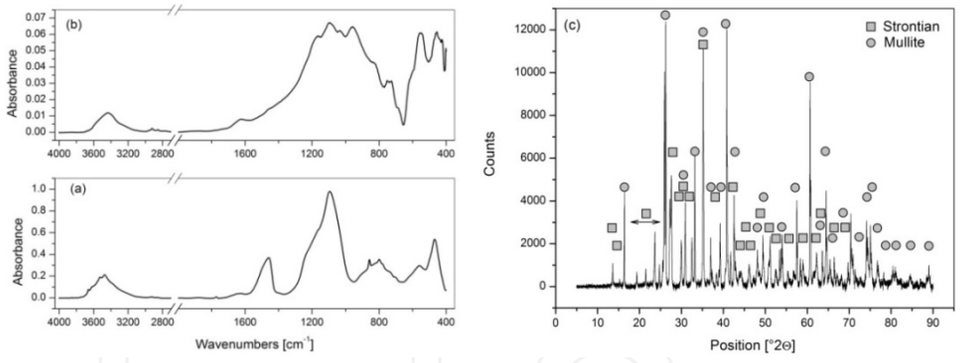


Figure 26. Infrared spectrum of raw foam (a), foam after the thermal treatment (b) and XRD of foam after the thermal treatment to 1500 °C (c).

After the thermal treatment (Fig.26(b)), the characteristic absorption bands of mullite ($3Al_2O_3$ $2SiO_2$) [583,588,589] and Sr-celsian, the Si-O stretching (1095 cm^{-1}) and bending (455 cm^{-1}) can be recognized in the spectra. The results of x-ray diffraction analysis (Fig.26(c)) confirm mullite and Sr-celsian as the main components in the sample.

4. MDF composites

Macro-defect-free (MDF) cements were developed by the research group led by Birchall at ICI during late 1970s and early 1980s [590]. MDF cements have unusual and superior properties

compared to traditional cement pastes and concretes, and are often referred to as chemically bound ceramics or MDF composites. The suggestions of applications of MDF cements are extremely wide ranging. These include roofing tiles, fire resistant doors, sewage pipes, airport bridges, window shutters, plastic moulds, printing rollers, thermal insulators, tube exhaust, oil tanks, corrosion resistant tanks, cable duct covers, electric generator propellers, electrical parts, boat decking, brake lining, body armor, pallets, toys, cryogenic vessels, signboards, cooler boxes, sound insulators and electromagnetic interference screenings [591,592].

However, after 25 years since they were first patented, the incorporation of MDF materials into commercial processes has been very limited. Despite the identification of many potential applications, MDF cements have certain limitations, in particular the loss of strength on exposure to moisture or humidity. The modifications of the MDF manufacturing process and the selection of polymer used have overcome many of these problems. The major obstacles restraining MDF cements from many applications are the economics of manufacturing on a large scale and their overall commercial viability compared to existing materials [591-593].

The manufacture of MDF cement involves high shear mixing of selected polymers and hydraulic cements at low *w/c* ratios typically between 0.08 and 0.20. The key stages of the typical MDF preparation process are shown in Fig. 27. Calcium aluminate cement (CAC), polyvinyl alcohol (PVA) and glycerol are the most applied input materials [12,592].

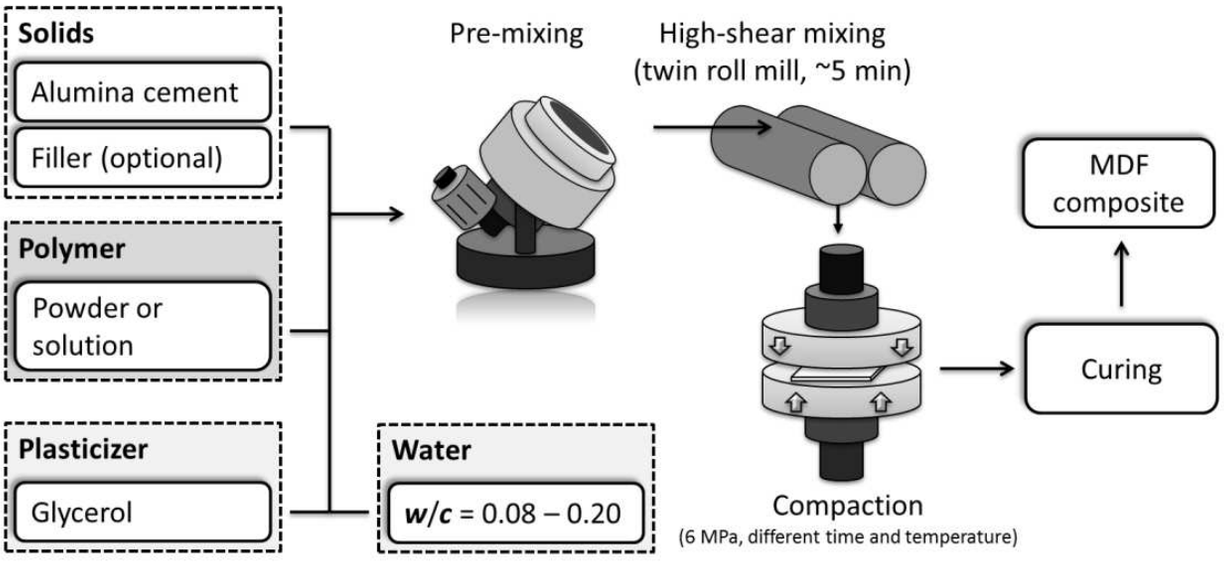


Figure 27. Typical stages of MDF manufacturing process [592].

MDF microstructure was described as close packed unhydrated cement grains within a three dimensional PVA network, with the coatings of hydrated cement on the surface, which interacts with the bulk polymer via chemical cross-linking. MDF cements comprise three distinct regions [592,594]:

a. **Unhydrated cement grains** due to the low *w/c* ratio there is a stoichiometric deficit of water that restrains all cement from full hydration;

b. Bulk polymer phase;

c. Complexinter-phase region which includes hydrated cement particles and polymer chains

A new alternative to MDF composites is the CAPR composites (Calcium Aluminate Phenol Resin), which are produced using the processing similar to that required for MDF cement manufacture (Fig.27). In CAPR composites high alumina cement (or other hydraulic cement) is mixed with a phenol resin precursor. A modifier is used to control the cross linking density and glycerol is added as a plasticizer. The process does not involve the addition of water and the cement is hydrated only by water given off by the phenol precursor during the condensation polymerization reaction that occurs in situ. This can lead to CAPR composites with an effective w/c ratio as low as 0.01 [592,595-597].

The formation of pastes in both systems is shown in Fig.28. Calcium-rich calcium aluminates, CaO, and $Ca(OH)_2$ showed high reactivity with phenol resin during roll milling while calcined alumina showed poor combining during roll milling. This indicates that Ca^{2+}ion is the reactive component whereas Al^{3+}ions control the excessive stiffness of the high alumina cement/phenol resin system.

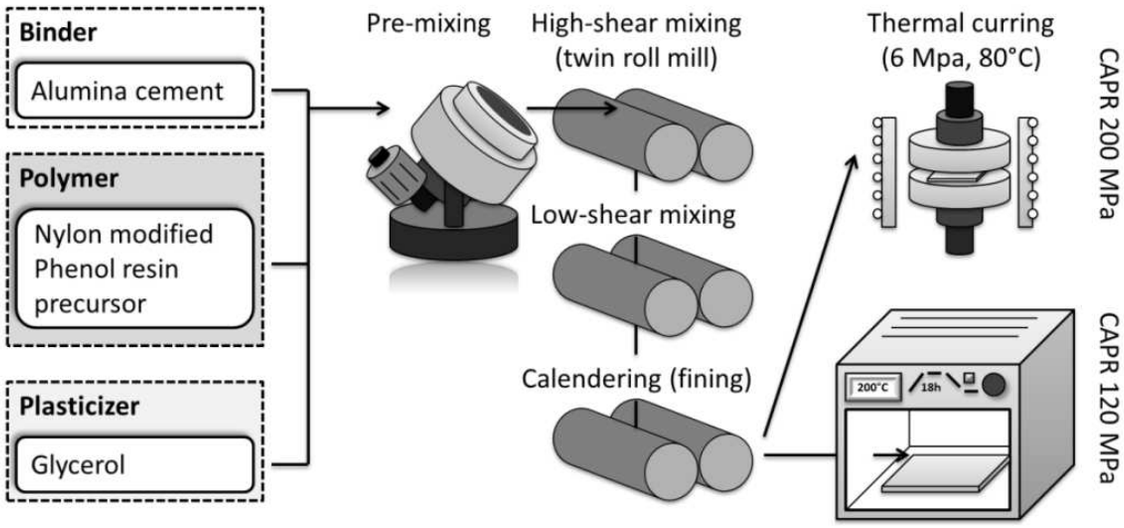


Figure 28. Flow chart of the preparation process of CAPR [595].

The formation of pastes in both systems is shown in Fig.29. Calcium-rich calcium aluminates, CaO, and $Ca(OH)_2$ showed high reactivity with phenol resin during roll milling while calcined alumina showed poor combining during roll milling. This indicates that Ca^{2+}ion is the reactive component whereas Al^{3+}ions control the excessive stiffness of the high alumina cement/phenol resin system.

Higher strength was achieved by Al^{3+}ion-rich calcium aluminate cements, and lower strength of calcium silicate based OPC indicates that the presence of Al^{3+}ions is essential for active thermal curing. On the basis of these observations, we suppose that the phenol resin precursor

cross-links with Ca^{2+}ions of cement through an ionic cross-linking reaction during the roll milling and then with Al^{3+}ions through a chemical cross-linking reaction during thermal curing [598].

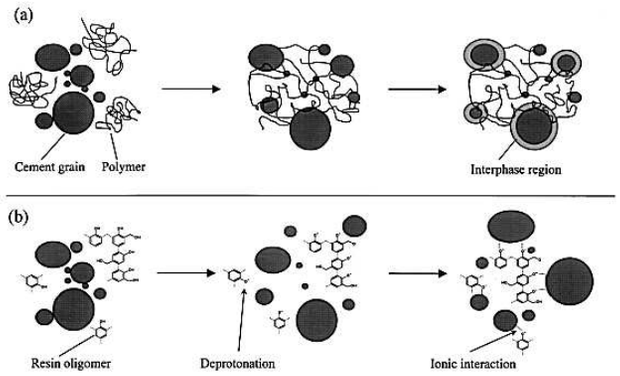


Figure 29. Mechanism of the paste formation of MDF system CA – PVA (a) and of CAPR composite (b) [597].

4.1. MDF composites based on strontium aluminate cement

MDF cement based on strontium aluminate is a promising material for the preparation of refractory products with thin wall and complicated shape. MDF composites based on strontium aluminate cement can be prepared by similar way as MDF cements based on calcium aluminate cement (Fig.27). A certain drawback is fast hydration of strontium aluminate cement, therefore the utilization of additives improving the workability of cement mixture with polymer and plasticizer is necessary.



Figure 30. Preparation of strontium aluminate based MDF using twin roll mixer.

The MDF material in Fig.30 is the first prepared sample of macro defect free composite based on strontium aluminate cement. It was prepared from the mixture of SrA cement, glycerol and PVA. After premixing of MDF components the mixing on twin roll mixer was performed. The sample compacted between two steel plates was then cured at the temperature of 60 °C.

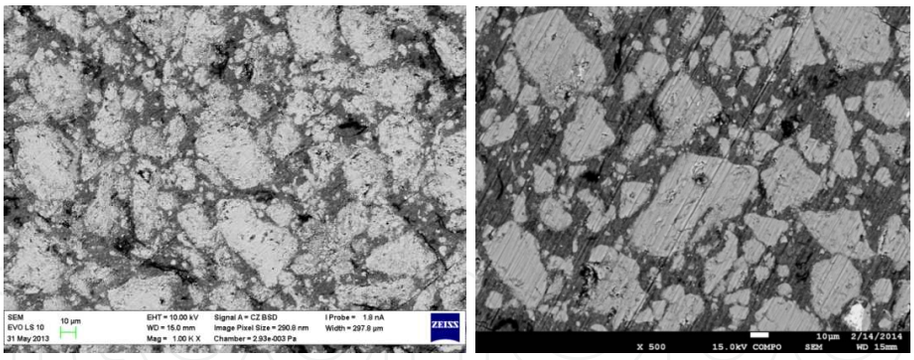


Figure 31. SEM analysis of MDF from strontium aluminate cement.

The SEM picture in the BSE-COMPO mode in Fig.31 shows the structure of prepared material where unhydrated grains of strontium aluminate cement were covered by the layer of hydration products. On the other hand the structure is not optimal due to fast hydration of strontium aluminate cement. Therefore, the additives improving cement workability are necessary in order to prepare MDF of higher quality. The other interesting options for the preparation of MDF should be the utilization of SrAC and CAC blend (Chapter 7.1.1) or the structural modification of the main clinker phase, e.g. by B_2O_3 (Chapter 7.3.2).

The preparation of shell of refractory product requires the thermal treatment to the temperatures, at which the ceramics bond is form. The behaviour of hydrated cement upon the thermal treatment is described in Chapter 6.5 and some properties of the product after the thermal treatment in Chapter 6.4.2.

4.2. Using MDF for refractory purposes

The options to use MDF composites prepared from strontium aluminate cement for refractory purposes require the information on the behaviour at high temperatures. High temperature heating microscopy performed up to the temperature of 1600 °C shows the thermal stability of MDF based on strontium aluminate cement (Fig.32).

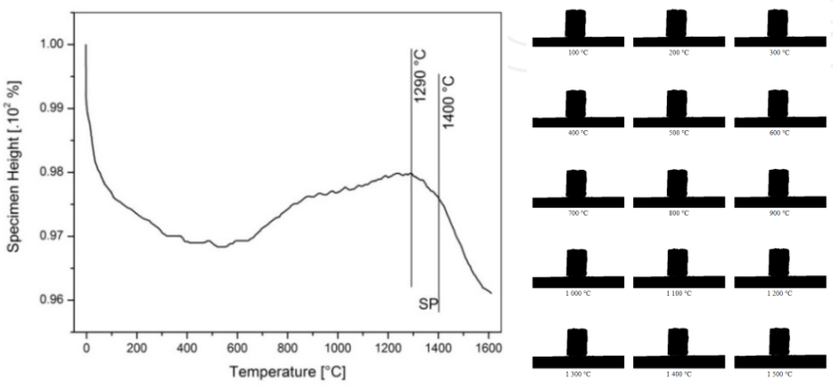


Figure 32. Heating microscopy of SrAC MDF specimen.

The initial shrinkage of specimen of about 3 % which takes place below the temperature of 600 °C is caused by the thermal decomposition of hydrates. The synthesis of strontium and tri-strontium aluminate from the product of dehydration and the thermal decomposition of strontium carbonate leads to the small expansion of 1 % within the temperature range from 650 to 900 °C. Up to the temperature of 1290 °C, the single thermal expansion of the sample takes place with the average thermal expansion coefficient of $1.073 \cdot 10^{-5}$ K^{-1}. The length contraction of sample occurs at temperatures higher than 1290 °C. The start of sintering was observed at the temperature of 1400 °C, but the change of height was still very small (about 2 %) at the temperature of 1600 °C.

The SEM image of MDF heated to the temperature of the start of sintering for 1 hour, where newly formed ceramic bond substitutes the hydraulic bond, which was lost during the thermal decomposition of hydrates (Chapter 6.5) is shown in Fig.33. The fracture area morphology shows the formation of necks (first stage sintering) between grains. In this stage, the material reaches the flexural strength of 14.6 MPa and the Young´s module of 5.2 GPa.

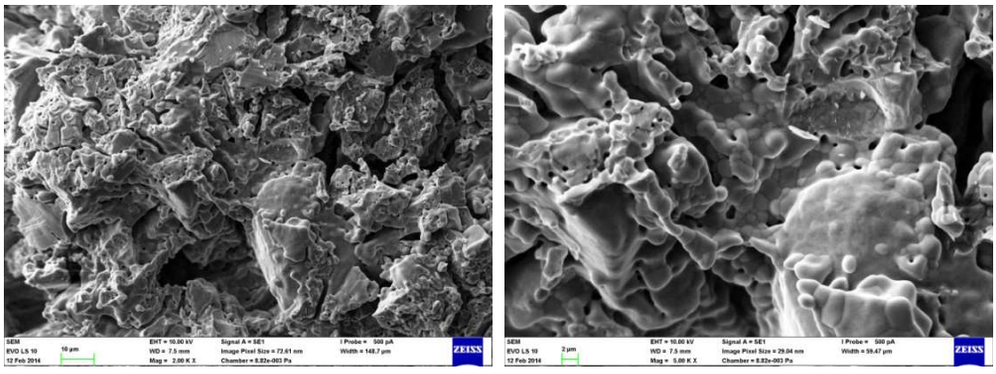


Figure 33. SEM image of fracture area of strontium aluminate MDF treated to the temperature of 1400 °C

5. Behaviour of hydrated cement stone during thermal treatment

The processes which take place during the thermal treatment of materials based on hardened strontium aluminate cement include the thermal decomposition of hydrates, repeated synthesis of strontium aluminate phases and sintering (formation of ceramic bond) in the case that material was treated to sufficient temperature. In the materials prepared with opening materials (aggregate) the newly formed phases appear. Their composition depends on the kind of applied aggregate.

The Kissinger plot related to the thermal decomposition of hydrates is shown in Fig.34. Table 4 summarizes the kinetic results of the behaviour of hardened strontium aluminate cement stone during the thermal treatment.

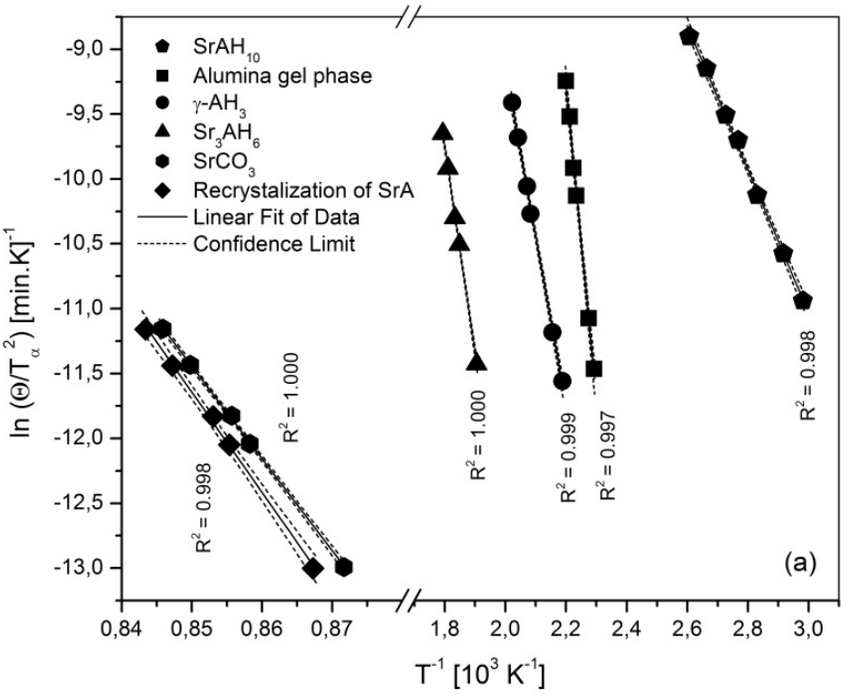


Figure 34. Kissinger plot [379].

Phase	E_a	A	α_m	$w_{1/2}$	n	The description of the mechanism of process
	[kJ•mol^{-1}]	[s^{-1}]	[%]	[°C]		
$SrAH_7$	46	$7.79 \cdot 10^5$	49.50	50.0	0.92	Growth of particles of appreciable initial volume, needles and plates of finite long dimensions.
AH_3 gel	200	$3.46 \cdot 10^{22}$	52.13	24.32	0.79	Growth of particles of appreciable initial volume, thickening of very large plates.
γ-AH_3	108	$1.45 \cdot 10^{22}$	50.48	9.14	4.18	Interface-controlled growth of a new phase, constant or increasing nucleation rate.
Sr_3AH_6	117	$3.94 \cdot 10^{10}$	49.70	17.75	2.54	Diffusion-controlled growth of a new phase, constant or increasing nucleation rate.
Sr	592	$2.28 \cdot 10^{24}$	46,11	19.31	2.31	Diffusion-controlled growth of a new phase, decreasing nucleation rate.
SrA	642	$4.30 \cdot 10^{26}$	54.25	17.95	2.48	Diffusion-controlled growth of a new phase, constant or decreasing nucleation rate.

Table 4. Mechanism and kinetics of thermal decomposition of hydration products.

The final product of the thermal treatment of hydrated cement stone is also strontium aluminate, i.e. the same compound as in the original clinker phase. Nevertheless it is formed through different reaction pathway compared to the original mixture of raw materials.

The thermal treatment of hydraulically bound refractory castables based on strontium aluminate cements leads to the thermal decomposition of hydrates. Disappearing of hydraulic bond naturally leads to decreasing strength, but bonding function is gradually adopted by ceramic bond formed with increasing temperature. The sintering of cement stone takes place at temperatures higher than 1400 °C (Fig.32) and the material becomes almost dehydrated at temperatures higher than 600 °C (Fig.35 and Fig.5 in Chapter 5). Therefore, there is a temperature range with significantly reduced strength.

The influence of temperature on to the equilibrium composition of hydrated cement stone with the composition corresponding to the 28th day of hydration process (Fig.2 in Chapter 5) is shown in Fig.35(a). The thermal treatment leads to the same compounds as the processing of strontium aluminate clinker from the mixture of raw materials (Fig.30 in Chapter 4). On the other hand, there is one significant difference, which is that the hydration process leads to better homogeneity than can be reached by the processing of raw material. That facilitates the solid state synthesis of clinker minerals.

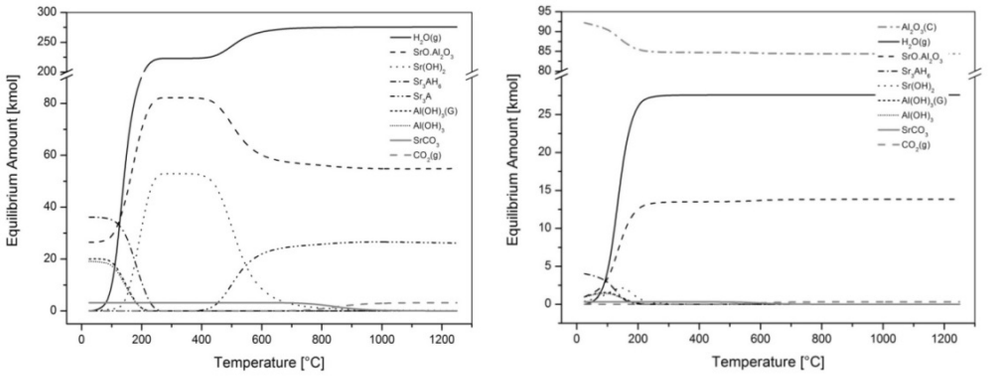


Figure 35. Effect of temperature on the equilibrium composition of hydrated cement stone (a) and hypothetical NCC (b).

The utilization of pure strontium aluminate cement without opening material (corundum, bauxite, mullite, fireclay, etc.) is not supposed, therefore Fig.35b shows the temperature evolution of equilibrium of refractory material in which the content of Al_2O_3 is increased to 90 % by the addition of alumina. These systems do not prefer the formation of tri-strontium aluminate.

The tri-strontium aluminate hexahydrate (Sr_3AH_6) is the main product of hydration of strontium aluminate cement. The thermal decomposition of analogical C_3AH_6 phase (Eqs.6 and 7), the calculation of the dependence of equilibrium composition on the temperature (Fig. 35) as well as the thermal analysis of hydrated samples (Figs.5 and 15(a) in Chapter 5) indicate the formation of strontium hydroxide during thermal decomposition of Sr_3AH_6. Assuming analogical thermals decomposition sequence as for C_3AH_6, it can be written as:

$$Sr_3AH_6 \rightarrow Sr_3AH_{1.5} + 4.5\ H \tag{51}$$

$$Sr_3AH_{1.5} \rightarrow anhydrou\ sphases + 1.5\ H \tag{52}$$

The theoretical mass loss on ignition for Sr_3AH_6 phase is 15.56+5.19=20.75 %. The mass loss of 15.36+4.98=20.34 % can be read from the first and second step of TG curve in Fig.15 in Chapter 5. That indicates that the thermal decomposition of tri-strontium aluminate hexahydrate can be described by Eqs.51 and 52. Therefore it should be written as:

$$7\ Sr_3AH_6 \rightarrow Sr_{12}A_7H + 9SrH + 32\ H. \tag{53}$$

IntechOpen
IntechOpen

IntechOpen

IntechOpen